Article

Cell

Lateral Inhibition in Cell Specification Mediated by Mechanical Signals Modulating TAZ Activity

Graphical Abstract

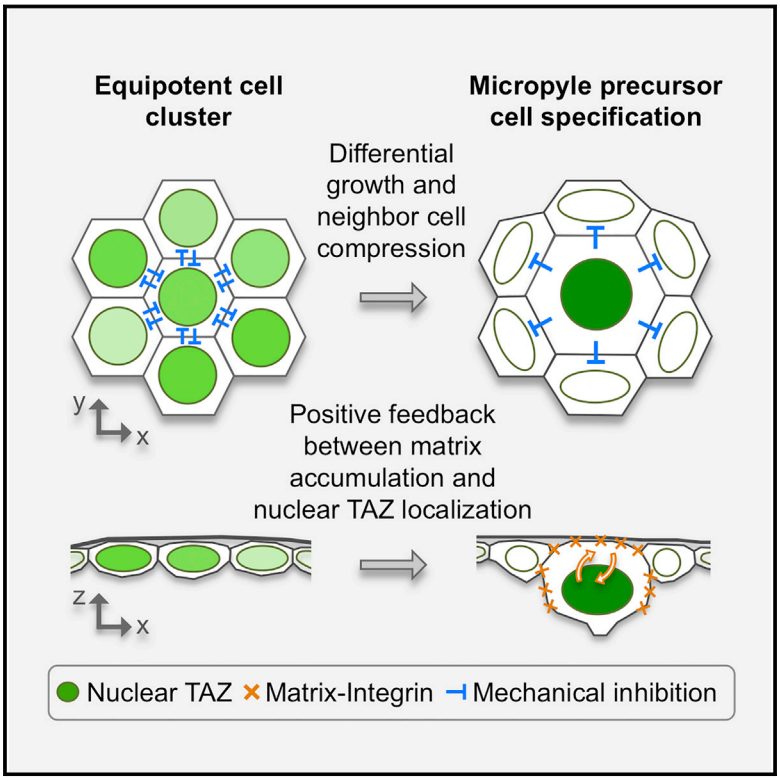

Authors

Peng Xia, Daniel Gütl, Vanessa Zheden, Carl-Philipp Heisenberg

Correspondence

heisenberg@ist.ac.at

In Brief

Specification of a single precursor cell fate in zebrafish oogenesis is mediated by lateral inhibition driven by mechanical forces that lead to nuclear exclusion of a developmental transcriptional activator in neighboring cells.

Highlights

- A single micropyle precursor cell (MPC) is specified within the granulosa cell layer
- MPC specification relies on lateral inhibition of neighboring cells
- Lateral inhibition is mediated by mechanical compression controlling nuclear TAZ
- TAZ hyperactivation in MPC requires positive feedback from extracellular matrix

Xia et al., 2019, Cell *176*, 1379–1392
March 7, 2019
https://doi.org/10.1016/j.cell.2019.01.019

CellPress

Cell

Lateral Inhibition in Cell Specification Mediated by Mechanical Signals Modulating TAZ Activity

Peng Xia,[1] Daniel Gütl,[1] Vanessa Zheden,[1] and Carl-Philipp Heisenberg[1,2,*]
[1]Institute of Science and Technology Austria, 3400 Klosterneuburg, Austria
[2]Lead Contact
*Correspondence: heisenberg@ist.ac.at
https://doi.org/10.1016/j.cell.2019.01.019

SUMMARY

Cell fate specification by lateral inhibition typically involves contact signaling through the Delta-Notch signaling pathway. However, whether this is the only signaling mode mediating lateral inhibition remains unclear. Here we show that in zebrafish oogenesis, a group of cells within the granulosa cell layer at the oocyte animal pole acquire elevated levels of the transcriptional coactivator TAZ in their nuclei. One of these cells, the future micropyle precursor cell (MPC), accumulates increasingly high levels of nuclear TAZ and grows faster than its surrounding cells, mechanically compressing those cells, which ultimately lose TAZ from their nuclei. Strikingly, relieving neighbor-cell compression by MPC ablation or aspiration restores nuclear TAZ accumulation in neighboring cells, eventually leading to MPC re-specification from these cells. Conversely, MPC specification is defective in *taz*$^{-/-}$ follicles. These findings uncover a novel mode of lateral inhibition in cell fate specification based on mechanical signals controlling TAZ activity.

INTRODUCTION

For a single cell to acquire a different developmental fate from its surrounding cells typically involves a mechanism commonly known as lateral inhibition (Perrimon et al., 2012). In lateral inhibition, first a group of cells is collectively determined to acquire a certain fate. The subsequent interaction between these initially equipotent cells leads to one dominant cell being singled out to acquire the primary cell fate, whereas the remaining cells of the group will eventually take on a secondary cell fate. For the dominant cell to be singled out, it needs to prevent primary fate acquisition in its direct neighbors via an inhibitory signal. Seminal studies on neurogenesis in both flies and vertebrates have identified Notch signaling as the inhibitory signal by which the dominant cell suppresses primary cell fate acquisition in neighboring cells (Lai, 2004). However, whether Notch is the sole signal mediating lateral inhibition remains unclear.

YAP and TAZ signaling has emerged as a major determinant of cell fate specification in development (Yu et al., 2015). During mammalian pre-implantation development, for instance, YAP and TAZ signaling activity determines whether cells become part of the inner cell mass or the trophectoderm (Nishioka et al., 2009). Several biochemical signals, most prominently components of the Hippo signaling pathway, have been implicated in modulating YAP and TAZ signaling activity by regulating their nuclear localization (Halder et al., 2012; Hansen et al., 2015). When in the nucleus, YAP and TAZ function as transcriptional co-activators, regulating the expression of a large number of target genes involved in cell fate specification, proliferation, and morphogenesis (Porazinski et al., 2015; Zanconato et al., 2015; Zhang et al., 2009). Not only biochemical but also mechanical signals, such as shear stress, extracellular matrix rigidity, and cell and/or nucleus deformation, have been shown to control YAP and TAZ activity (Dupont et al., 2011; Elosegui-Artola et al., 2017; Wang et al., 2016). How those mechanical signals exert their effects on YAP and TAZ nuclear localization is not yet entirely understood, but mechanosensation at cell-cell and cell-matrix adhesion sites is thought to translate into changes of the actomyosin network, which again affect YAP and TAZ nuclear localization (Dupont et al., 2011).

In zebrafish oogenesis, the granulosa cell layer surrounding the maturing oocyte triggers formation of the chorion, an acellular eggshell surrounding the developing oocyte (Selman et al., 1993). The chorion contains a particular structure, the micropyle, which, during fertilization, functions as a channel to guide sperm from the outside to the mature oocyte (Yanagimachi et al., 2013). Micropyle formation has been traced back to a single cell within the granulosa cell layer, the micropyle precursor cell (MPC) (Selman et al., 1993; see also Figure 1A for a schematic representation of the MPC and surrounding tissue during oogenesis). Moreover, MPC specification has previously been linked to animal-vegetal polarization of the oocyte, with the MPC being located above the animal pole of the oocyte (Marlow and Mullins, 2008). However, the molecular and cellular mechanisms underlying MPC specification within the granulosa cell layer during oocyte maturation remain unknown.

RESULTS

Fast-Growing MPC Mechanically Compresses Its Neighboring Granulosa Cells

Previous studies have identified a single MPC within the granulosa cell layer surrounding the oocyte in stage III ovarian follicles (Selman et al., 1993; see also Figure 1A). To obtain insight into the molecular and cellular mechanisms underlying MPC fate determination, we analyzed the ultra-structural composition of

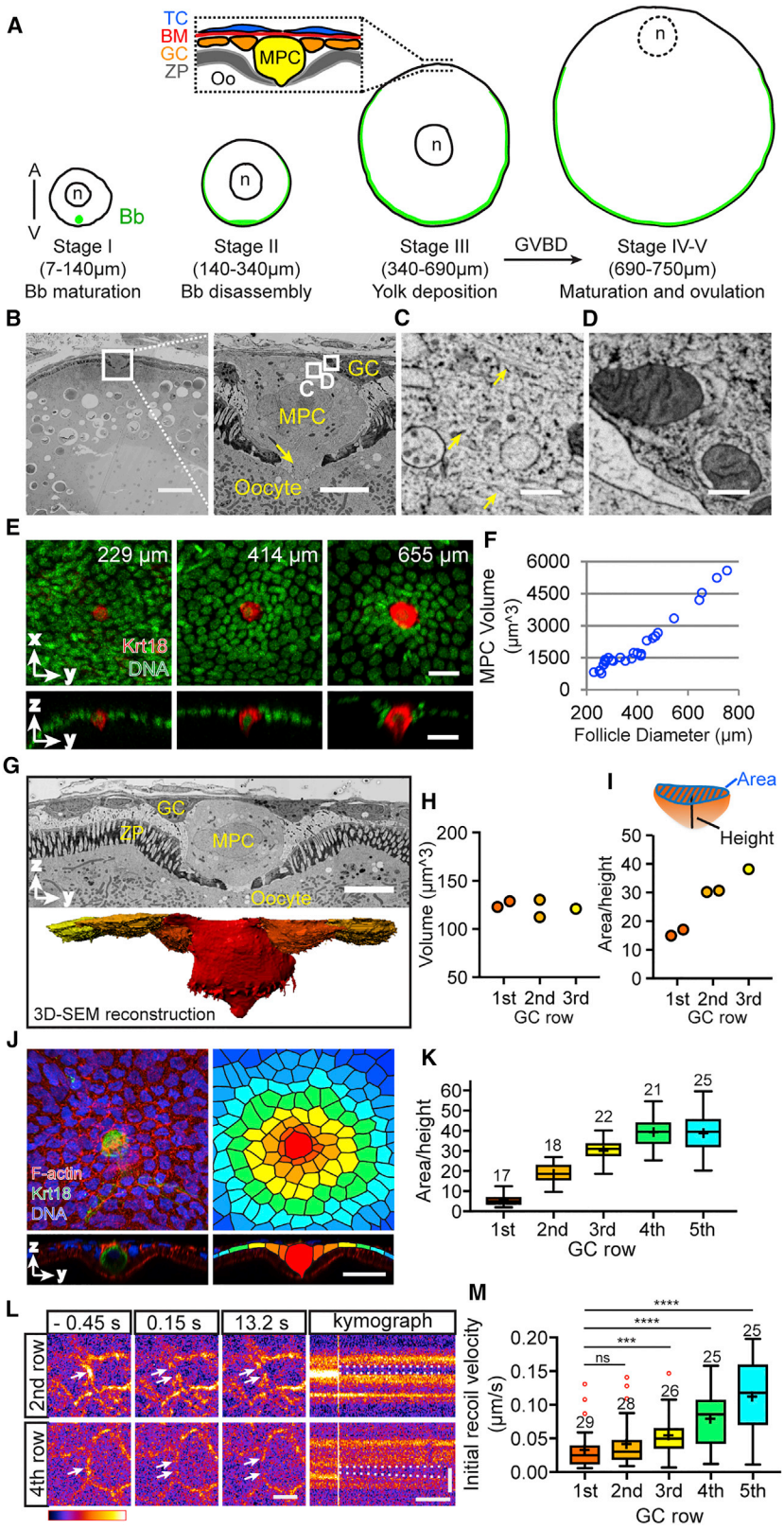

Figure 1. The MPC Mechanically Compresses Surrounding Granulosa Cells

(A) Schematic representation of ovarian follicle development from stage I to stage V. Green labels the Balbiani body (Bb, in stage I) or Bb components (after stage II). The boxed region in stage III shows the MPC within the animal pole of the follicle. MPC, micropyle precursor cell; TC, theca cell; BM, basement membrane; GC, granulosa cell; ZP, *zona pellucida*; Oo, oocyte; GVBD, germinal vesicle breakdown.

(B) Scanning electron microscopy (SEM) images of a stage II follicle (318-µm diameter). Left: low-magnification view of the animal pole; scale bar, 30 µm. Right: high-magnification view of the MPC within the boxed area outlined on the left side; the yellow arrow points to a protrusion from the MPC toward the oocyte; scale bar, 5 µm.

(C and D) High-magnification views of the boxed areas outlined in (B), right. The yellow arrows in (C) point to filamentous structures with a diameter of ≈10 nm found in the MPC (C) but not the adjacent granulosa cells (D), indicative of intermediate filament accumulation within the MPC. Scale bars, 0.3 µm.

(E) Confocal images of Krt18 expression in MPCs and granulosa cells at the animal pole of follicles with a diameter of 229 µm (left column), 414 µm (center column), and 655 µm (right column) showing the accumulation of Cytokeratin 18 (Krt18) within the MPC, visualized by immunohistochemistry. Cell nuclei are marked by DAPI. Shown at the top are maximum-intensity projection (MIP) planar x,y views, and shown at the bottom are y,z cross-sections along a horizontal line passing through the center of the MPC. Scale bars, 20 µm.

(F) Plot of MPC volume as a function of changes in follicle diameter during follicle maturation. Data are from 30 follicles of 3 animals.

(G) SEM image (top) and 3D-SEM reconstruction (bottom) of the MPC with surrounding granulosa cells. Note the dense array of microvilli passing through the zona pellucida and directly connecting the oocyte with the MPC and granulosa cells. Color coding of cells corresponds to color coding of the cell rows in (J, right). Scale bar, 5 µm.

(H and I) Volume (H) and area-to-height ratio (I) of granulosa cells in the first 3 cell rows surrounding the MPC obtained from the 3D-SEM reconstruction (G, bottom). See also (J) for positioning of the granulosa cell rows surrounding the MPC. Color-coding of the points refers to color-coding of the cell rows in (J, right). The schematic above (I) shows how granulosa cell height and area were defined.

(J) Confocal image (left) and image segmentation (right) of the MPC and surrounding granulosa cells at the animal pole of late stage II follicles (270–330 µm). The cell cortex is marked by Phalloidin-Rhodamine-labeled F-actin, cell nuclei by DAPI, and the MPC by Krt18 immunohistochemistry. Different rows of granulosa cells surrounding the MPC are color-coded. Shown at the top are MIP planar x,y views, and shown at the bottom are y,z cross-sections along a horizontal line passing through the center of the MPC. Scale bar, 20 µm.

(K) Area to height ratio of granulosa cells in different rows surrounding the MPC obtained from confocal images as shown in (J, left). Color-coding of plot boxes refers to color-coding of the cell rows in (J, right). Values

(legend continued on next page)

the MPC in late stage II follicles using scanning electron microscopy (SEM). Consistent with previous observations (Selman et al., 1993), we found the MPC to be considerably bigger than its immediate neighbors and to be directly connected to the underlying oocyte via a large protrusion containing microtubule-like structures (Figures 1B, S1A, and S1B). Interestingly, we also found cytoskeletal elements resembling intermediate filaments specifically accumulating in the MPC (Figures 1C and 1D), suggesting that intermediate filaments might be involved in MPC differentiation. To test this possibility, we analyzed the expression of Cytokeratin18 (Krt18), one of the most commonly expressed intermediate filaments (Pan et al., 2013), in the MPC at different stages of follicle maturation using immunohistochemistry. Taking advantage of oocytes that express GFP-tagged Bucky ball (Buc) to mark the vegetal pole (Bontems et al., 2009), we observed elevated expression of Krt18 but not other Keratins such as Krt4 (Figure S1C), in a single granulosa cell located close to the animal pole of the oocyte from early oogenesis (early-middle stage II) onward (Figures 1E). This cell—judged by its position (Figure S1D), fast growth, and unique morphology (Figures 1E and 1F)—appeared to be the MPC. Interestingly, this MPC-like cell also expressed elevated levels of phospho-S6 (Figures S1E and S1F), a characteristic marker for activation of the mTOR pathway, previously associated with cell growth (Saxton and Sabatini, 2017). To confirm whether the Krt18-expressing cell identified indeed is the MPC, we turned to *buc* mutants, which had previously been shown to form multiple MPCs within the ovarian follicle because of failed animal-vegetal polarization of the oocyte (Dosch et al., 2004; Marlow and Mullins, 2008). In stage II–III follicles of *buc* mutants, there were multiple single granulosa cells distributed over the entire granulosa cell layer that displayed the characteristic morphology of MPCs and expressed high levels of Krt18 (Figures S1G and S1H). This supports the notion that Krt18 expression is an early marker for MPC differentiation. Importantly, although we found several single Krt18-positive MPCs in *buc* mutants, we never observed multiple MPCs that were located directly adjacent to each other (Figures S1G and S1H). This points to the intriguing possibility that MPC specification may involve some form of lateral inhibition, preventing immediate neighbors from acquiring the same fate.

To address this possibility, we first determined how the MPC interacts with its neighboring cells during follicle maturation using high-resolution confocal imaging and 3D SEM images. We found that, from stage II onward, granulosa cells directly neighboring the MPC became increasingly compacted and adopted a deformed shape indicative of mechanical compression by the expanding MPC (Figures 1G–1K and S1I). Analyzing shape changes of the MPC and its neighbors during stage II revealed two concomitant morphogenetic processes leading to this arrangement: first, the MPC grew bigger, increasing its volume more than four times (Figures 1E–1G); second, the neighboring granulosa cells kept their volume constant and became more compacted and deformed relative to the expanding MPC (Figures 1G–1K and S1I). This combination of events is consistent with a model where differential growth between the MPC and its surrounding granulosa cells generates pushing forces emanating from the growing MPC and compressing its immediate neighboring granulosa cells. To directly test this model, we used a *krt18:krt18-GFP* transgenic line allowing us to identify and monitor the MPC in live follicles (Figure S1J). Using this line, we then performed UV laser ablation of cell-cell junctions between granulosa cells in the vicinity of the MPC at late stage II to reveal tension distribution within the granulosa cell layer. We reasoned that if there would be pushing forces generated by the differential growth between the MPC and its surrounding granulosa cells, then tension should decrease at neighboring granulosa cell-cell junctions that are oriented perpendicular to the MPC surface and that this effect should be more evident close to the MPC than farther away. For analyzing junctional tension, we made use of a UV laser cutting setup and determined the recoil velocity of junctions after UV laser cutting as a readout of their tension (Behrndt et al., 2012). This analysis revealed that tension at junctions oriented orthogonal to the MPC between granulosa cells directly adjacent to the MPC was significantly smaller than between granulosa cells located farther away from the MPC (Figures 1L and 1M). Altogether, these findings support the notion that the expanding MPC mechanically compresses its neighboring granulosa cells.

Nuclear TAZ Differentially Accumulates in the MPC and Its Neighboring Granulosa Cells

Given that the differentiation of a single MPC coincided with the expanding MPC mechanically compressing its neighboring cells, it is conceivable that the MPC suppresses MPC specification in its immediate neighbors by eliciting a mechanosensitive response in those cells. YAP and TAZ signaling has previously been implicated in mechanosensation (Dupont et al., 2011), and we thus asked whether YAP and TAZ might also be involved in MPC specification. Taking advantage of an antibody specifically detecting TAZ in zebrafish (Miesfeld et al., 2015; Figure S2A), we analyzed TAZ localization in granulosa cells of stage II follicles. We found that, at early stage II, a small group of granulosa cells (2–5) at the animal pole began to express higher levels of TAZ

are shown as Tukey box-and-whisker plots with median (bar) and average values (cross). Sample size (cells) is indicated over each box; data are from 6 late stage II (270–330 μm) follicles of 3 animals.

(L) Spinning disk confocal images of representative cell-cell junctions between granulosa cells in the second (top) and fourth row (bottom) surrounding the MPC in late stage II follicles subjected to UV laser cutting. Junctions are shown before (−0.45 s) and after (0.15 s and 13.2 s) cutting. Cuts were 3 μm long and were all performed on junctions oriented perpendicular to the MPC. Junctions were cut at 0 s. Arrows indicate cut region and junction opening. Scale bar, 5 μm. Right: kymographs showing the evolution of junction opening following the cut. Junction openings are outlined by dashed white lines. Horizontal scale bar, 5 s. Perpendicular scale bar, 5 μm.

(M) Analysis of initial recoil velocities for laser cuts in the first 5 rows of granulosa cells surrounding the MPC. Values are shown as Tukey box-and-whisker plots with median (bar) and average values (cross). Sample size (cuts) is indicated over each box; data are from 133 follicles of 14 animals. Statistical test, Mann-Whitney *U* test, two tailed. ns, not significant; ***$p < 0.001$; ****$p < 0.0001$.

See also Figure S1.

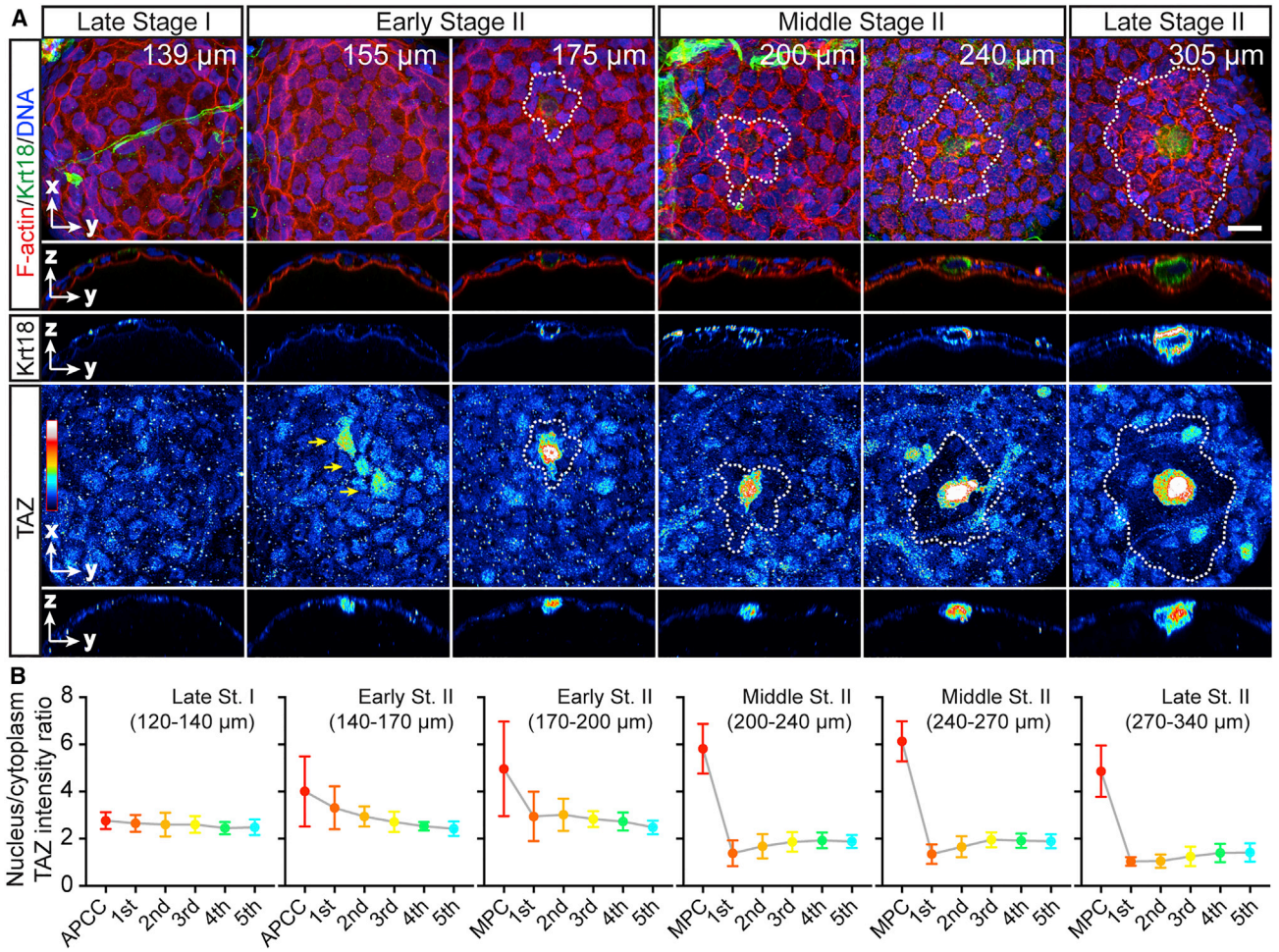

Figure 2. TAZ Nuclear Localization in the MPC and Surrounding Granulosa Cells

(A) Confocal images of cells at the animal pole of stage I–II follicles stained for the cell cortex by Phalloidin-Rhodamine-labeled F-actin, cell nuclei by DAPI, Krt18 (top 3 rows), and TAZ (bottom two rows) by immunohistochemistry. The first and fourth rows are MIP planar x,y views, and the second, third, and fifth rows are y,z cross-sections along a horizontal line passing through the center of the MPC. The stage of follicle maturation is indicated by follicle diameter in the top right corner. Yellow arrows in the TAZ image of the 155-μm follicle indicate 3 granulosa cells at the animal pole with higher TAZ nuclear intensity. The regions of granulosa cells surrounding the MPC and showing clearly reduced TAZ nuclear intensity are outlined with dashed white lines. Scale bar, 15 μm.

(B) Nucleus to cytoplasm TAZ intensity ratio in the MPC (when it is detectable at early stage II) and surrounding GCs in stage I–II follicles. Before the MPC became detectable (late stage I to early stage II), the cell at the center of the animal pole (APCC) was quantified relative to the surrounding granulosa cells instead of the MPC. Values are shown as mean (dot) and SD (whisker). Data are from 4 follicles for late stage I (120–140 μm), 6 for early stage II (140–170 μm), 11 for early stage II (170–200 μm), 10 for middle stage II (200–240 μm), 8 for middle stage II (240–270 μm), and 16 for late stage II (270–340 μm); follicles were collected from 6 animals. For each follicle, around 80 cells were analyzed.

See also Figures S2 and S3.

than their immediate neighbors (Figures 2A and 2B). This was specific to the animal pole because no such group of cells could be identified in other positions of the oocyte, such as the vegetal pole (Figures S2B and S2C). Shortly after (early to middle stage II), this elevated nuclear localization of TAZ became restricted to a single granulosa cell at the animal pole, that displayed the characteristic morphology of the MPC (Figure 2A). Notably, granulosa cells neighboring the MPC showed even less TAZ nuclear localization than granulosa cells farther away from the MPC (Figure 2A), giving rise to a pattern of TAZ nuclear localization at the animal pole of early to middle stage II oocytes where the MPC displaying very high levels of nuclear TAZ was surrounded by 1–3 rows of granulosa cells showing very low levels of nuclear TAZ that, again, were surrounded by granulosa cells further away from the MPC showing slightly higher levels of nuclear TAZ (Figures 2A and 2B). Moreover, comparing deformation of granulosa cells surrounding the MPC at middle stage II with their TAZ nuclear localization showed a close inverse relationship between the degree of granulosa cell deformation by the MPC and their level of nuclear TAZ accumulation (Figure S2D).

The selection of a single MPC showing very high levels of nuclear TAZ from early to middle stage II appeared to be a stepwise process, where an increasingly smaller number of cells were showing an increasingly higher level of nuclear TAZ; eventually,

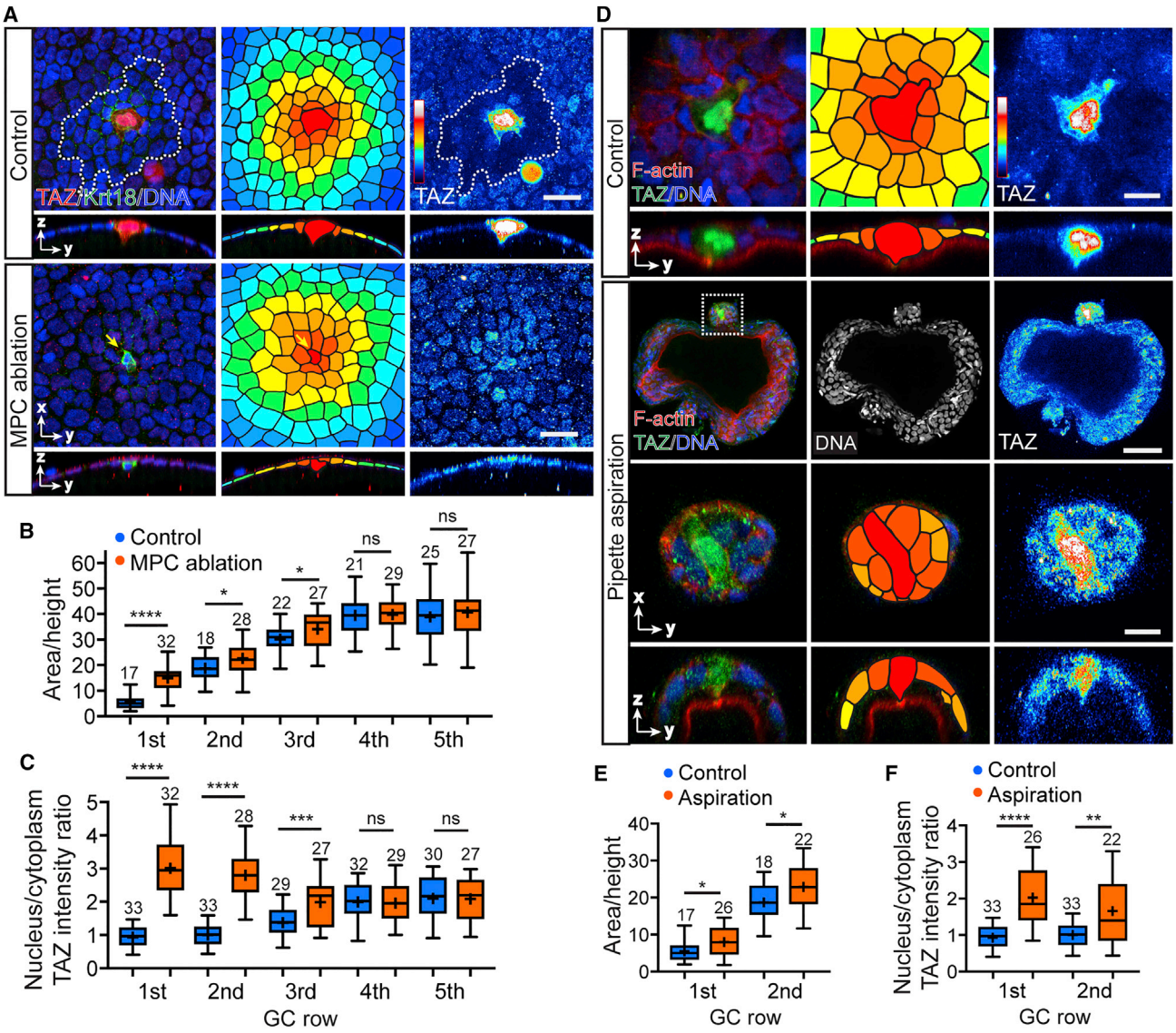

Figure 3. MPC Reduces TAZ Nuclear Localization in Surrounding Granulosa Cells by Mechanical Compression

(A) Confocal images (left and right columns) and image segmentation (center column) of MPCs and granulosa cells (GC) at the animal pole of late stage II follicles in the presence (top two rows, control) or absence (bottom two rows, MPC laser ablation) of the MPC. Samples were fixed 6 h after laser ablation. MPCs and surrounding granulosa cells are labeled by their expression of Krt18-GFP, cell nuclei by DAPI, and TAZ by immunohistochemistry. Yellow arrows demarcate ablated MPCs. The bright dot in the bottom right corner of the top row is an out-of-plane unspecific fluorescence signal. Shown in the top row are maximun intensity projection (MIP) planar x,y views, and shown in the bottom row are y,z cross-sections along a horizontal line passing through the center of the MPC. Regions of granulosa cells surrounding the MPC and showing clearly reduced TAZ nuclear intensity are outlined with dashed white lines. Scale bars, 20 μm.

(B and C) Area to height ratio (B) and nucleus to cytoplasm TAZ intensity ratio (C) of granulosa cells in control and MPC-ablated follicles in different rows surrounding the MPC obtained from confocal images. Values are shown as Tukey box-and-whisker plots with median (bar) and average values (cross). Sample size (cells) is indicated over each box; data are from 10 late stage II follicles of 3 animals (for control and MPC ablation experiments each). Statistical test, Mann-Whitney *U* test, two tailed. *p < 0.05, ***p < 0.001, ****p < 0.0001.

(D) Confocal images (left and right columns) and image segmentation (center column) of MPC and granulosa cells at the animal pole of follicles without micropipette aspiration (top 2 rows) or after aspiration (bottom 3 rows). Follicles were fixed after 1.5 h of aspiration. The cell cortex is marked by Phalloidin-Rhodamine-labeled F-actin, cell nuclei by DAPI, and TAZ by immunohistochemistry. Controls are 2.5-μm optical section MIP planar x,y views (top row of controls) and lateral 2.5-μm optical sections along a horizontal line passing through the center of the MPC (bottom row of controls). In images of samples after aspiration, the top row shows low-magnification, 20-μm optical section MIP views of the follicle, with the aspirated region outlined by the boxed area on the left. In the row below (center row) are 2.5-μm optical section MIP high-magnification views at the animal pole of the aspirated region outlined by the boxed area in the top row. In the bottom row are 2.5-μm optical section MIP lateral views of the aspirated region outlined by the boxed area in the top row. Scale bars, 50 μm (third row) and 20 μm (first and fourth rows).

(legend continued on next page)

this led to one single granulosa cell displaying very high levels of TAZ, accompanied by a pronounced reduction of TAZ nuclear localization in the neighboring cells (Figures S3A and S3B). Interestingly, this evolution of nuclear TAZ level in granulosa cells at the animal pole of oocytes from early-to-middle stage II follicles was closely mirrored by changes in granulosa cell size and Krt18 expression, where the granulosa cells displaying increasingly high levels of nuclear TAZ also showed a tendency to increase their size and expression of Krt18 (Figures S3A–S3C). Collectively, these observations point to the possibility that TAZ signaling is involved in MPC specification and further suggest a model whereby the expanding MPC might inhibit TAZ nuclear localization and, thus, MPC specification in neighboring cells by mechanically compressing them.

MPC Suppresses Nuclear TAZ Accumulation in Neighboring Granulosa Cells by Mechanically Compressing Them

To test whether mechanical compression by the expanding MPC indeed represents the critical signal regulating TAZ nuclear localization in neighboring cells, we ablated the MPC cell in late stage II follicles using a UV laser. Remarkably, shortly (6 h) after MPC ablation, neighboring granulosa cells not only appeared less deformed and compacted than before (Figures 3A and 3B) but also displayed clearly increased levels of nuclear TAZ when compared not only with their levels before ablation but also with granulosa cells farther away from the ablated MPC (Figures 3A and 3C). This suggests that neighboring granulosa cells after MPC ablation regain elevated levels of nuclear TAZ localization, indicative of early stages of MPC specification. To exclude that the effect of MPC ablation on nuclear TAZ localization is due to interference with biochemical signals from the MPC directly controlling TAZ nuclear localization in its neighboring cells, we also directly relieved compression of the neighboring granulosa cells and analyzed the resultant changes in nuclear TAZ localization. For relieving neighboring granulosa cell compression, we stretched the granulosa cell layer by either aspirating the MPC and surrounding granulosa cells into a micropipette (Figures 3D and 3E; note that both the MPC and surrounding granulosa cells had to be aspirated to effectively relieve compression of granulosa cells by the MPC) or ablating a few granulosa cells next to the MPC (Figures S4A and S4B). Similar to the MPC ablation experiments, the neighboring granulosa cells in both the granulosa cell ablation and aspiration experiments not only became less deformed and compacted but also showed clearly elevated levels of TAZ in their nuclei, indicative of early stages of MPC specification (Figures 3E, 3F, S4B, and S4C).

TAZ Is Required for MPC Specification

To determine whether neighboring cells regaining elevated levels of nuclear TAZ after MPC ablation would be able to form a new MPC, as expected for a lateral inhibition process underlying MPC specification, we followed the fate of these cells over 4 days in culture. Remarkably, we found that a similar selection process leading to MPC specification was activated in these cells, as observed in granulosa cells at the animal pole at early to middle stage II (Figures 2 and S3). First, a small group of granulosa cells surrounding the ablation site began to display increasingly higher levels of TAZ in their nuclei, eventually leading to one granulosa cell showing very high levels of TAZ in its nucleus, and the cells directly surrounding it showing reduced TAZ nuclear localization (Figures 4A and 4B). The "winning" cell not only showed very high levels of nuclear TAZ but also displayed all features typically associated with an MPC, such as its characteristic size and shape, with a large protrusion marked by elevated levels of acetylated tubulin and F-actin, which was in direct contact with the underlying oocyte (Figures 4A–4F). Moreover, this cell, much like the original MPC before ablation, expressed strongly elevated levels of marker proteins delineating MPC specification and differentiation, such as Krt18 and phospho-S6 (Figures 4A, 4E, and 4G). Collectively, these findings suggest that MPC specification involves simultaneous upregulation of TAZ activity in the expanding MPC and downregulation of TAZ activity in the neighboring granulosa cells triggered by cell deformation by the MPC.

To determine whether TAZ activity is also required for micropyle formation, we generated maternal zygotic (MZ) *taz* mutant females (Miesfeld and Link, 2014) and analyzed whether micropyle formation is affected in their follicles. Oocytes from MZ*taz* mutant females displayed a highly abnormal micropyle structure in their chorion and, given the essential function of the micropyle in channeling the sperm through the chorion to the oocyte, could not be fertilized (Figures 5A–5D). In contrast, oocytes from MZ mutant females of the TAZ ortholog YAP (Miesfeld et al., 2015) showed a normal micropyle in their chorion (Figures S5A and S5B), suggesting that YAP, in contrast to TAZ, is not required for micropyle formation. To test whether TAZ is also involved in MPC specification, we analyzed follicles from MZ*taz* mutant females and found that there was no clearly recognizable compaction of granulosa cells at the animal pole of the oocyte as seen in wild-type (WT) follicles (Figures 5E and 5F), and none of the granulosa cells in MZ*taz* follicles displayed the characteristic size, shape, Krt18 expression, and phospho-S6 activation of an MPC at a comparable stage of oogenesis in WT (Figures 5G–5J). Moreover, comparing the general level of Krt18 expression in granulosa cells between WT and MZ*taz* mutant follicles showed clearly reduced levels in mutant follicles, suggesting that TAZ is generally required for Krt18 expression in granulosa cells (Figures S5C and S5D). In contrast, the overall animal-vegetal polarity of the oocyte as well as granulosa cell density and total cell number remained largely unchanged in stage II *MZtaz* mutant follicles (Figures S5E–S5H). Collectively, these observations suggest that TAZ activity is essential for MPC specification but dispensable for oocyte polarization

(E and F) Area to height ratio (E) and nucleus to cytoplasm TAZ intensity ratio (F) of granulosa cells in control and aspirated follicles. Values are shown as Tukey box-and-whisker plots with median (bar) and average values (cross). Sample size (cells) is indicated over each box; data are from 10 follicles of 3 animals (for control and aspiration experiments each). Statistical test, Mann-Whitney *U* test, two tailed. *$p < 0.05$, **$p < 0.01$, ****$p < 0.0001$.
See also Figure S4.

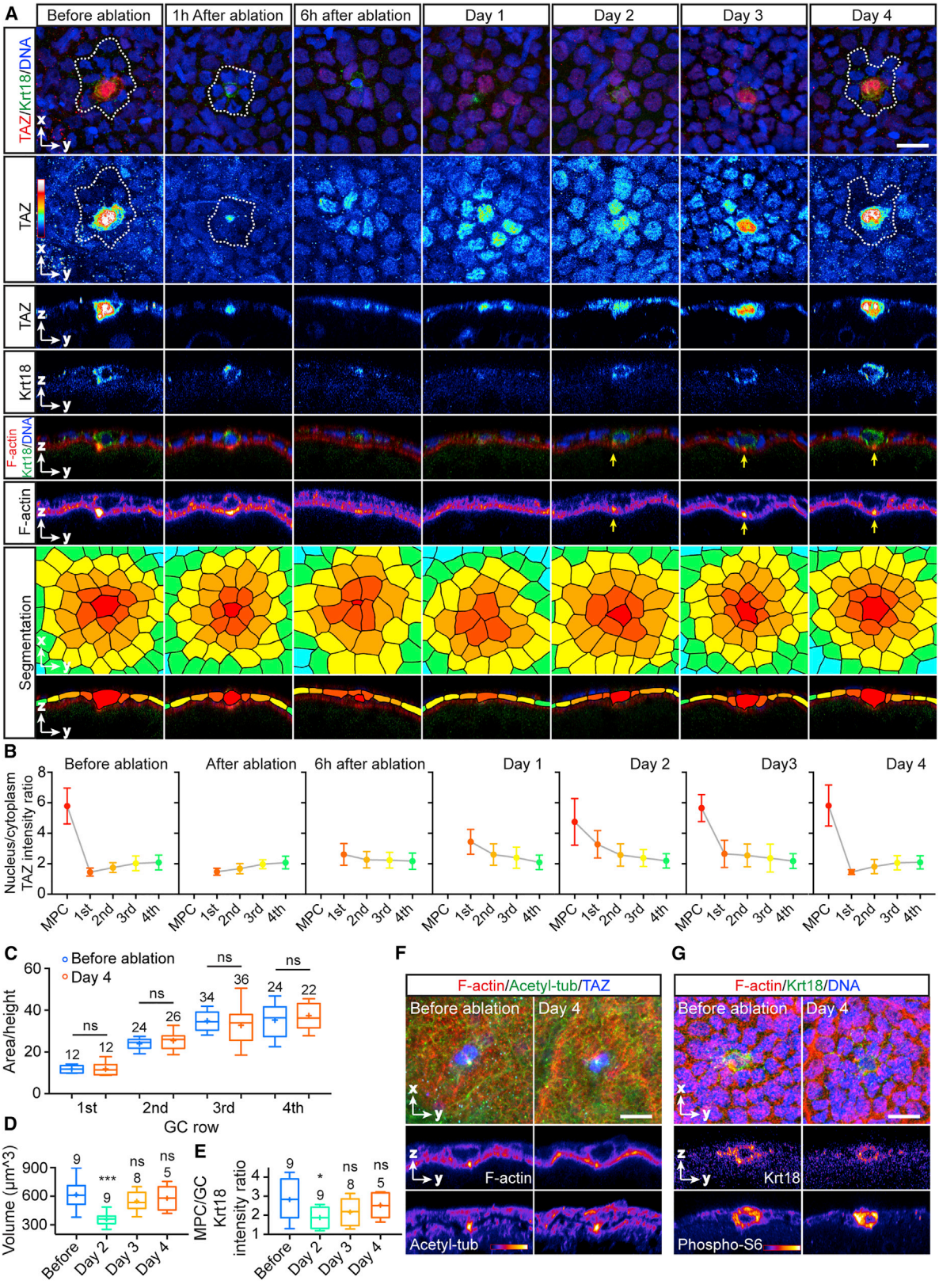

(legend on next page)

and granulosa cell proliferation during early stages of MPC specification.

Hyper-activation of TAZ in the MPC Depends on Positive Feedback from Cell-Matrix Adhesion

Our data so far support a model where the growing MPC inhibits MPC specification in neighboring granulosa cells by downregulating TAZ activity through mechanical compression. However, questions remain regarding the mechanisms driving hyper-activation of TAZ in the MPC itself. The TAZ ortholog YAP has previously been shown to promote its own activity by engaging in a positive feedback loop, where YAP triggers the expression of proteins involved in cell-matrix adhesion, and cell matrix adhesion activates YAP (Calvo et al., 2013). To test whether such a positive feedback loop might also be involved in TAZ hyper-activation in the MPC, we analyzed the expression and subcellular localization of several potential target genes of YAP and TAZ (Porazinski et al., 2015; Zanconato et al., 2015; Zhang et al., 2009) implicated in the regulation of cell-matrix adhesion in stage II follicles. Among those target genes, we found strongly elevated levels of Integrin β1 at the plasma membrane in lateral portions of the MPC (Figure 6A). This accumulation was first observed after early stage II, when TAZ expression and nuclear localization had already been established in the MPC, and was absent in late stage II follicles from *taz* mutant females, supporting the notion that Integrin β1 accumulation within the MPC is under the control of TAZ (Figures 6A and 6B). Interestingly, we also found extracellular matrix (ECM) components, such as Fibronectin and Laminin, to accumulate at basal and lateral regions of the MPC in WT but not *taz* mutant oocytes (Figures 6C–6F), suggesting that the maturing MPC becomes tightly attached to the surrounding ECM by Integrin-to-ECM adhesions.

Activation of Src tyrosine kinase signaling by Integrin-to-ECM adhesion has previously been implicated in promoting YAP and TAZ activity (Elbediwy and Thompson, 2018; Elbediwy et al., 2016; Kim and Gumbiner, 2015). To determine whether the contact of the MPC to the surrounding ECM is required to maintain high TAZ activity in the MPC, we sought to interfere with MPC-to-ECM adhesion and analyze resultant changes in TAZ activity. To globally reduce cell adhesion, we exposed late stage II oocytes to 10–100 mM EDTA, which depletes Ca^{2+} from the medium and interferes with cadherin-mediated cell-cell and Integrin-mediated cell-matrix adhesion. MPCs exposed to EDTA rounded up and displayed strongly reduced contacts to both the adjacent granulosa cells and surrounding ECM (Figures S6A and S6B). Interestingly, even short (3 h) exposure to EDTA was sufficient to elicit this phenotype and also led to strongly diminished nuclear localization of TAZ in the MPC (Figures S6A and S6B). To more specifically interfere with Integrin-to-ECM adhesion, we treated late stage II follicles with 2 mg/mL RGD peptides and monitored the resultant effects on TAZ nuclear localization in the MPC. TAZ nuclear localization was already clearly reduced in the MPC 8 h after RGD peptide treatment (Figures 7A and 7B), suggesting that Integrin-to-ECM adhesion is required for TAZ hyper-activation in the MPC. Finally, to determine how Integrin-to-ECM adhesion triggers TAZ nuclear localization in the MPC, we exposed middle to late stage II follicles to drugs inhibiting different effector proteins shown previously to function as signaling mediators of Integrin-to-ECM adhesion (Giancotti and Ruoslahti, 1999). We found that inhibiting the activities of FAK, Src, phosphatidylinositol 3-kinase (PI3K), and PDK1 for 8 h led to a significant reduction of nuclear TAZ within the MPC, suggesting that these molecules function as effector proteins of Integrin-to-ECM adhesion, promoting TAZ hyperactivation in the MPC (Figures 7C, 7D, S6C, and S6D). In contrast, inhibition of ERK, AKT, and mTOR had less significant effects on TAZ nuclear localization in the MPC, arguing against a critical function of these molecules in regulating TAZ nuclear localization downstream of Integrin-to-ECM adhesion within the MPC (Figures 7C, 7D, S6C, and S6D). Collectively, these observations suggest that hyper-activation of TAZ in the MPC relies on a positive feedback loop of TAZ promoting Integrin-to-ECM adhesion and Integrin-to-ECM adhesion promoting TAZ nuclear localization by activating a downstream signaling pathway involving FAK, Src, PI3K, and PDK1 (Figure 7E).

Figure 4. MPC Suppresses MPC Specification in Surrounding Granulosa Cells

(A) Confocal images of MPCs and granulosa cells (GC) at the animal pole of early to middle stage II follicles (190–230 μm) before (first column) and after (second through seventh columns) MPC ablation, stained for TAZ by immunohistochemistry, cell nuclei by DAPI, Krt18 by transgenic Krt18-GFP expression (top 4 rows), and cell cortex by Phalloidin-Rhodamine-labeled F-actin (fifth and sixth rows). The bottom two rows are image segmentations. The top two rows are maximum intensity projection (MIP) planar x,y views, and the third through sixth rows are y,z cross-sections along a horizontal line passing through the center of the MPC. The duration of follicle culturing relative to MPC ablation is indicated on top of each column. Yellow arrows in columns 5–7 and rows 5 and 6 (F-actin images of days 2–4) demarcate MPC protrusion toward the oocyte. The regions of granulosa cells that surround the MPC and show clearly reduced TAZ nuclear intensity are outlined with dashed white lines. Scale bar, 15 μm.

(B) Nucleus to cytoplasm TAZ intensity ratio in the MPC and surrounding granulosa cells before and after MPC ablation. Values are shown as mean (dot) and SD (whisker). Data are from 9 (before ablation), 4 (1 h after ablation), 5 (6 h after ablation), 5 (day 1), 9 (day 2), 8 (day 3), and 5 (day 4) follicles of 12 animals. For each follicle, around 20 cells were analyzed.

(C) Area to height of granulosa cells before and 4 days after MPC ablation. Values are shown as Tukey box-and-whisker plots with median (bar) and average values (cross). Sample size (cells) is indicated over each box; data are from 5 animals. Statistical test, Mann-Whitney *U* test, two tailed.

(D and E) MPC volume (D) and MPC to granulosa cell Krt18 intensity ratio (E) in follicles before MPC ablation and 2–4 days after ablation. Values are shown as Tukey box-and-whisker plots with median (bar) and average values (cross). Sample size (cells) is indicated over each box; data are from 12 animals. Statistical test was performed between each group (after ablation) and the control group (before ablation), Mann-Whitney *U* test, two tailed. The p values are indicated above the sample sizes; *$p < 0.05$, ***$p < 0.001$.

(F and G) Confocal images of MPCs and granulosa cells at the animal pole of early to middle stage II follicles before MPC ablation (left column) and 4 days thereafter (right column). Cell nuclei are marked by DAPI, F-actin by Phalloidin-Rhodamine, TAZ, acetylated tubulin (F), and phospho-S6 (G) by immunohistochemistry, and Krt18 (G) by transgenic Krt18-GFP expression. Shown at the top are MIP planar x,y views, and shown at the bottom are y,z cross-sections along a horizontal line passing through the center of the MPC. Scale bars, 15 μm.

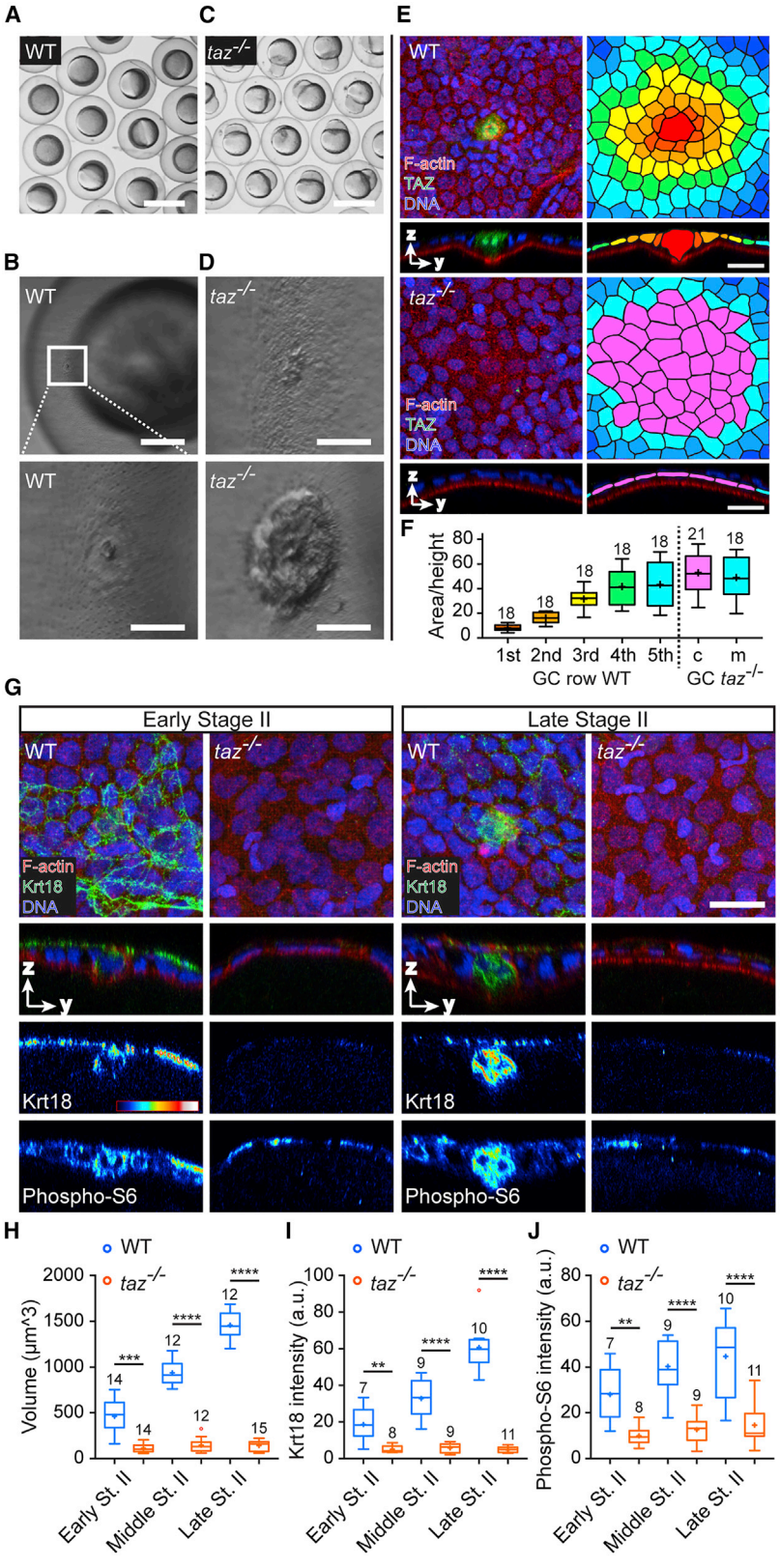

Figure 5. TAZ Is Required for MPC Specification and Surrounding Granulosa Cell Compaction

(A) Bright-field image of fertilized embryos generated by WT females crossed with *taz* homozygous males. Scale bar, 1 mm.

(B) Low-magnification (top) and high-magnification bright-field images (bottom) of the micropyle region (boxed area at the top) within the chorion of an embryo generated by WT females crossed with *taz* homozygous males. Scale bars, 200 µm (top) and 50 µm (bottom).

(C) Bright-field image of unfertilized embryos generated by *taz* homozygous females crossed with WT males. Scale bar, 1 mm.

(D) High magnification bright-field images of the micropyle region in embryos generated by *taz* homozygous females crossed with WT males. Left and right: different micropyle phenotypes. Scale bar, 50 µm.

(E) Confocal images (left column) and image segmentation (right column) of MPCs and granulosa cells (GC) at the animal pole of late stage II follicles from WT (top 2 rows) and *taz* homozygous females (bottom 2 rows). Cell nuclei are marked by DAPI, F-actin by Phalloidin-Rhodamine, and TAZ by immunohistochemistry. In the WT, different rows of granulosa cells surrounding the MPC are color-coded. For *taz* homozygous follicles, granulosa cells at the animal pole were subdivided into a center area of the same size as granulosa cell rows 1–4 in the WT and a marginal area corresponding to rows 5–7 in the WT. Shown in the top row are MIP planar x,y views, and shown in the bottom row are y,z cross-sections along a horizontal line passing through the center of the MPC or center of the central area. Scale bar, 20 µm.

(F) Area to height ratio of granulosa cells in different rows surrounding the MPC obtained from confocal images as shown in (E). The color-coding of the plot boxes refers to the color-coding of the cells in (E). For *taz* homozygous follicles, data of the center area are labeled as "c" and of the marginal area as "m." Values are shown as Tukey box-and-whisker plots with median (bar) and average values (cross). Sample size (cells) is indicated over each box; data are from 7 late stage II follicles of 3 animals (WT) and 6 late stage II follicles of 3 animals (*taz* homozygous).

(G) Confocal images of MPCs and granulosa cells at the animal pole of early stage II (left two columns) and late stage II (right two columns) follicles from WT (first and third columns) and *taz* homozygous females (second and fourth columns). Cell nuclei are marked by DAPI, F-actin by Phalloidin-Rhodamine, and Krt18 and phospho-S6 by immunohistochemistry. Shown at the top are MIP planar x,y views, and shown at the bottom are y,z cross-sections along a horizontal line passing through the center of the MPC or center of the central area. Scale bars, 15 µm.

(H–J) Volume (H), Krt18 intensity (I), and phospho-S6 intensity (J) of MPCs (in WT follicles) and animal pole center cells (in *taz* homozygous follicles) at early (140–200 µm), middle (200–270 µm), and late (270–340 µm) stage II. Values are shown as Tukey box-and-whisker plots with median (bar) and average values (cross). Sample size (cells) is indicated over each box; data are from 4 (WT) and 3 (*taz* homozygous) animals. Statistical test, Mann-Whitney *U* test, two tailed. $^{**}p < 0.01$, $^{***}p < 0.001$, $^{****}p < 0.0001$.

See also Figure S5.

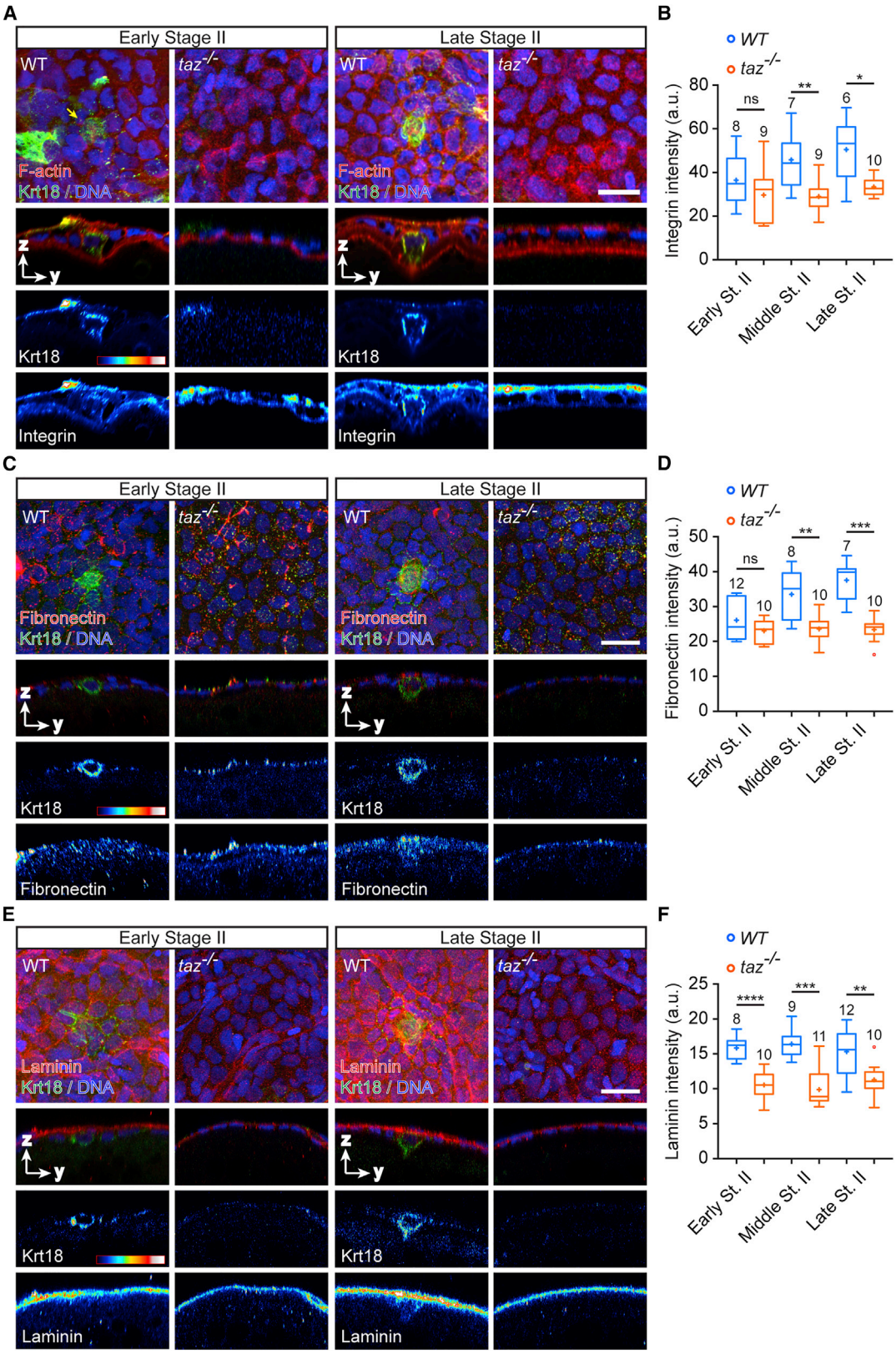

(legend on next page)

DISCUSSION

Here we show that lateral inhibition leading to specification of a single MPC within the zebrafish ovarian follicle is achieved by the inhibition of TAZ signaling in the neighboring cells (Figure 7E). Notably, the primary inhibitory signals in this case appears to be pushing forces by the dominant cell deforming its neighboring cells. These pushing forces are generated by TAZ-dependent differential growth between the dominant cell and its neighboring cells and elicit a mechanosensitive response in the neighboring cells that eventually is translated into an intracellular biochemical signal inhibiting TAZ nuclear accumulation. How mechanical signals modulate YAP and TAZ nuclear localization in the neighboring cells is not yet entirely clear, but modification of the actomyosin cytoskeleton, and cell/nucleus shape changes might be involved (Dupont et al., 2011; Elosegui-Artola et al., 2017; Meng et al., 2018; Porazinski et al., 2015).

Importantly, although our data suggest a critical function of mechanosensitive TAZ signaling in lateral inhibition leading to MPC specification, it does not exclude additional contributing mechanisms, such as biochemical signaling from the dominant cell. The finding that the effect of the dominant cell on TAZ nuclear localization in its neighboring cells is detectable several cell rows away from the dominant cell (Figure 2A and 2B), together with our observation that inhibition of Notch signaling, previously thought to be the prime signal mediating lateral inhibition (Lai, 2004), does not affect the general pattern of TAZ nuclear localization within the MPC and surrounding cells (Figures S7A and S7B), argues against Notch-mediated contact signaling playing a decisive role therein. This notion is further corroborated by our observation that Notch signaling is reduced in granulosa cells neighboring the MPC compared with the MPC itself (Figures S7C and S7D), opposite to what would be expected if Notch signaling would mediate lateral inhibition from the MPC in surrounding cells. Still, there might be other, not yet identified signaling pathways mediating lateral inhibition by the MPC. Our observation that reducing neighbor cell compression leads to increased nuclear TAZ localization in these cells and, eventually, to the specification of a new MPC suggests that mechanical pushing forces are required for the MPC suppressing nuclear TAZ localization and MPC specification in these cells. This, however, does not exclude that other inhibitory signals emitted by the MPC might function in conjunction with mechanical pushing forces in preventing neighboring cells from acquiring the same fate.

Oogenesis in zebrafish has only begun to be elucidated. Although there has been major progress in identifying the molecular and cellular mechanisms underlying oocyte polarization (Elkouby et al., 2016), remarkably little is known about how granulosa cells surrounding the oocyte develop and contribute to oocyte maturation. Our findings reveal that MPC specification within the granulosa cell layer is under the control of TAZ activity. How TAZ activity controls MPC specification and differentiation is still unclear, but the upregulation of Integrin adhesion molecules and intermediate filaments, such Cytokeratin 18, might play an important role. In fact, both Integrins and Cytokeratin 18 have previously been identified as transcriptional targets of YAP and TAZ (Meng et al., 2018; Zanconato et al., 2015; Zhang et al., 2009), suggesting that they could function as direct downstream effectors of YAP and TAZ signaling. Moreover, our observation that Integrin-mediated adhesion of the MPC to the ECM is required for sustained TAZ activity within the MPC points to a positive feedback mechanism whereby TAZ controls Integrin expression and Integrin-ECM adhesion controls TAZ activation.

Questions also remain regarding how the initial activation of TAZ in a small group of granulosa cells at the animal pole of the oocyte in early stage II follicles is established. The finding that in *buc*-mutant follicles, where the animal identity of oocytes is expanded, multiple MPCs are induced within the granulosa cell layer suggests that signals emerging from the animal pole of the oocyte might induce this precursor cell population (Marlow and Mullins, 2008). The nature of such a signal is not yet known, but given that mRNAs of *taram-a* and *vg1*, two well-described components of the Nodal (transforming growth factor β [TGF-β]) signaling pathway (Aoki et al., 2002; Fleming et al., 2013; Montague and Schier, 2017), have been shown to localize at the animal pole of the maturing oocyte (Bally-Cuif et al., 1998), it is conceivable that TGF-β signals might be involved.

Lateral inhibition in cell fate specification typically involves contact signaling through the Delta-Notch signaling pathway (Perrimon et al., 2012). Our finding of mechanosensitive TAZ signaling mediating lateral inhibition during MPC specification not just adds a new signaling pathway to this process but identifies mechanical pushing forces as a primary signal involved in lateral inhibition. Mechanical compression of cells has previously been proposed to induce cell fate specification in both vertebrate and invertebrate development by modulating β-catenin signaling (Brunet et al., 2013; Desprat et al., 2008). Our findings show that cell compression can also be used to inhibit primary cell fate specification and that changes in TAZ activity mediate this effect. This points to cell compression as a highly versatile signal influencing

Figure 6. TAZ Is Required for Integrin Expression and Extracellular Matrix Accumulation

(A, C, and E) Confocal images of Integrin (A), Fibronectin (C), and Laminin (E) expression in MPCs and granulosa cells at the animal pole region in early stage II (left two columns) and late stage II (right two columns) follicles from WT (first and third columns) and *taz* homozygous females (second and fourth columns). Cell nuclei are marked by DAPI, F-actin by Phalloidin-Rhodamine, Krt18 (A), Integrin β1, Fibronectin, Laminin by immunohistochemistry, and Krt18 (C and E) by transgenic Krt18-GFP expression. Shown at the top are maximum intensity projection (MIP) planar x,y views, and shown at the bottom are y,z cross-sections along a horizontal line passing through the center of the MPC or center of the central area. The yellow arrow in the first column (A) indicates the MPC. The bright staining of Krt18 in the bottom left corner in column 1 and row 1 is an out-of-plane unspecific fluorescence signal (A). Scale bars, 15 μm (A) and 20 μm (C and E).

(B, D, and F) Integrin (B), Fibronectin (D), and Laminin labeling intensity (F) in MPCs (in WT follicles) and animal pole center cells (in *taz* homozygous follicles) at early (140–200 μm), middle (200–270 μm), and late (270–340 μm) stage II. Values are shown as Tukey box-and-whisker plots with median (bar) and average values (cross). Sample size (cells) is indicated over each box; data are from 8 (WT) and 6 (*taz* homozygous) animals. Statistical test, Mann-Whitney *U* test, two tailed. *$p < 0.05$, **$p < 0.01$, ***$p < 0.001$, ****$p < 0.0001$.

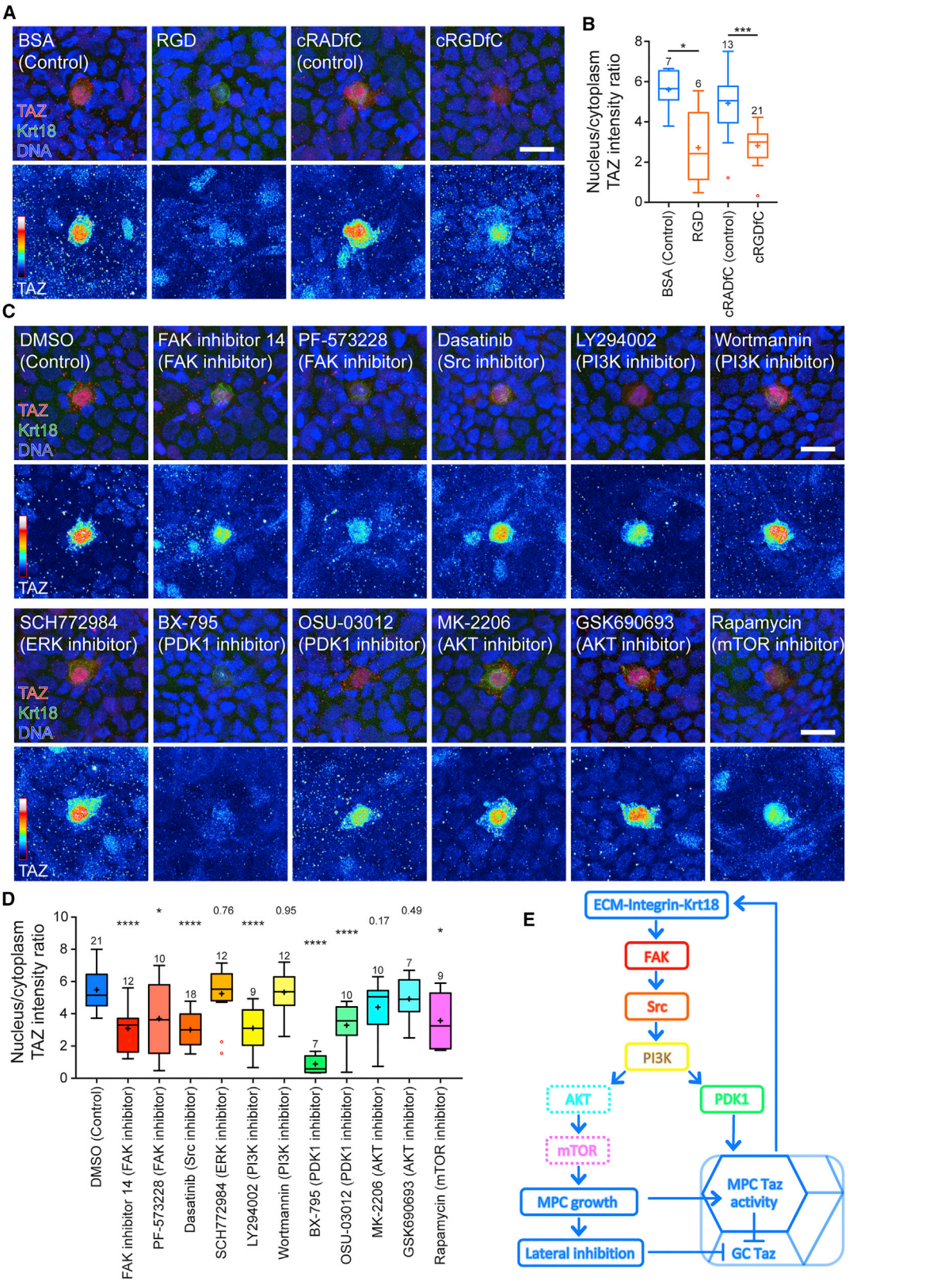

(legend on next page)

cell fate specification by regulating different mechanosensitive effector pathways.

STAR★METHODS

Detailed methods are provided in the online version of this paper and include the following:

- KEY RESOURCES TABLE
- CONTACT FOR REAGENT AND RESOURCE SHARING
- EXPERIMENTAL MODEL AND SUBJECT DETAILS
- METHOD DETAILS
  - Ovarian Follicle Isolation
  - Scanning Electron Microscopy
  - Brigh-field Imaging
  - Phalloidin, DAPI and Immunohistochemistry
  - Confocal Imaging
  - Analysis of Cell Volume and Area versus Height Value
  - Analysis of Fluorescent Intensity
  - Analysis of Granulosa Cell Density and Number
  - Tissue Tension Measurements
  - Cell Ablation Experiments
  - Follicle Aspiration Experiments
  - Drug Treatments
- QUANTIFICATION AND STATISTICAL ANALYSIS

SUPPLEMENTAL INFORMATION

Supplemental Information includes seven figures and can be found with this article online at https://doi.org/10.1016/j.cell.2019.01.019.

ACKNOWLEDGMENTS

We thank Roland Dosch, Makoto Furutani-Seiki, Brian Link, Mary Mullins, and Masazumi Tada for providing transgenic and/or mutant zebrafish lines; Alexandra Schauer, Shayan Shami-Pour, and the rest of the Heisenberg lab for technical assistance and feedback on the manuscript; and the Bioimaging, Electron Microscopy, and Zebrafish facilities of IST Austria for continuous support. This work was supported by an ERC advanced grant (MECSPEC to C.-P.H.).

AUTHOR CONTRIBUTIONS

P.X. and C.-P.H. designed the research. P.X. performed the experiments and analyzed the experimental data. D.G. and V.Z. helped with electron microscopy. P.X. and C.-P.H. wrote the manuscript.

DECLARATION OF INTERESTS

The authors declare no competing interests.

Received: May 1, 2018
Revised: October 18, 2018
Accepted: January 10, 2019
Published: February 14, 2019

REFERENCES

Aoki, T.O., Mathieu, J., Saint-Etienne, L., Rebagliati, M.R., Peyriéras, N., and Rosa, F.M. (2002). Regulation of nodal signalling and mesendoderm formation by TARAM-A, a TGFbeta-related type I receptor. Dev. Biol. *241*, 273–288.

Bally-Cuif, L., Schatz, W.J., and Ho, R.K. (1998). Characterization of the zebrafish Orb/CPEB-related RNA binding protein and localization of maternal components in the zebrafish oocyte. Mech. Dev. *77*, 31–47.

Behrndt, M., Salbreux, G., Campinho, P., Hauschild, R., Oswald, F., Roensch, J., Grill, S.W., and Heisenberg, C.-P. (2012). Forces driving epithelial spreading in zebrafish gastrulation. Science *338*, 257–260.

Bontems, F., Stein, A., Marlow, F., Lyautey, J., Gupta, T., Mullins, M.C., and Dosch, R. (2009). Bucky ball organizes germ plasm assembly in zebrafish. Curr. Biol. *19*, 414–422.

Brunet, T., Bouclet, A., Ahmadi, P., Mitrossilis, D., Driquez, B., Brunet, A.-C., Henry, L., Serman, F., Béalle, G., Ménager, C., et al. (2013). Evolutionary conservation of early mesoderm specification by mechanotransduction in Bilateria. Nat. Commun. *4*, 2821.

Calvo, F., Ege, N., Grande-Garcia, A., Hooper, S., Jenkins, R.P., Chaudhry, S.I., Harrington, K., Williamson, P., Moeendarbary, E., Charras, G., and Sahai, E. (2013). Mechanotransduction and YAP-dependent matrix remodelling is required for the generation and maintenance of cancer-associated fibroblasts. Nat. Cell Biol. *15*, 637–646.

Desprat, N., Supatto, W., Pouille, P.-A., Beaurepaire, E., and Farge, E. (2008). Tissue deformation modulates twist expression to determine anterior midgut differentiation in Drosophila embryos. Dev. Cell *15*, 470–477.

Dosch, R., Wagner, D.S., Mintzer, K.A., Runke, G., Wiemelt, A.P., and Mullins, M.C. (2004). Maternal control of vertebrate development before the midblastula transition: mutants from the zebrafish I. Dev. Cell *6*, 771–780.

Dupont, S., Morsut, L., Aragona, M., Enzo, E., Giulitti, S., Cordenonsi, M., Zanconato, F., Le Digabel, J., Forcato, M., Bicciato, S., et al. (2011). Role of YAP/TAZ in mechanotransduction. Nature *474*, 179–183.

Elbediwy, A., and Thompson, B.J. (2018). Evolution of mechanotransduction via YAP/TAZ in animal epithelia. Curr. Opin. Cell Biol. *51*, 117–123.

Elbediwy, A., Vincent-Mistiaen, Z.I., Spencer-Dene, B., Stone, R.K., Boeing, S., Wculek, S.K., Cordero, J., Tan, E.H., Ridgway, R., Brunton, V.G., et al. (2016). Integrin signalling regulates YAP and TAZ to control skin homeostasis. Development *143*, 1674–1687.

Figure 7. Integrin-to-Extracellular Matrix Adhesion Is Required for TAZ Hyper-activation within the MPC

(A) MIP confocal images of MPCs and granulosa cells (GC) at the animal pole of middle to late stage II follicles exposed to BSA (5 mg/mL) or the indicated RGD or control peptides (2 mg/mL) for 8 h. Cell nuclei are labeled by DAPI, TAZ by immunohistochemistry, and Krt18 by transgenic Krt18-EGFP expression. Scale bar, 15 μm.

(B) Nucleus to cytoplasm TAZ intensity ratio in MPCs exposed to BSA (5 mg/mL) or the indicated RGD or control peptides (2 mg/mL) for 8 h. Values are shown as Tukey box-and-whisker plots with median (bar) and average values (cross). Sample size (cells) is indicated over each box; data are from middle to late stage II follicles of 6 animals. Statistical testing was performed between the treatment group and the corresponding control group; Mann-Whitney *U* test, two tailed. *$p < 0.05$, ***$p < 0.001$.

(C) Maximum intensity projection (MIP) confocal images of MPC and granulosa cells at the animal pole of middle to late stage II follicles exposed to DMSO (control) or the indicated inhibitors for 8 h. Cell nuclei are labeled by DAPI, TAZ by immunohistochemistry, and Krt18 by transgenic Krt18-EGFP expression. Scale bars, 15 μm.

(D) Nucleus to cytoplasm TAZ intensity ratio in MPCs exposed to DMSO (control) or the indicated inhibitors for 8 h. Values are shown as Tukey box-and-whisker plots with median (bar) and average values (cross). Sample size (cells) is indicated over each box; data are from middle to late stage II follicles of 12 animals. Statistical testing was performed between each treatment group and the DMSO control; Mann-Whitney *U* test, two tailed. Non-significant p values are indicated above the sample sizes; *$p < 0.05$; ****$p < 0.0001$.

(E) Schematic of potential signals and/or signaling pathways mediating the effect of ECM on TAZ activation and MPC growth.

See also Figures S6 and S7.

Elkouby, Y.M., and Mullins, M.C. (2017). Methods for the analysis of early oogenesis in Zebrafish. Dev. Biol. *430*, 310–324.

Elkouby, Y.M., Jamieson-Lucy, A., and Mullins, M.C. (2016). Oocyte Polarization Is Coupled to the Chromosomal Bouquet, a Conserved Polarized Nuclear Configuration in Meiosis. PLoS Biol. *14*, e1002335.

Elosegui-Artola, A., Andreu, I., Beedle, A.E.M., Lezamiz, A., Uroz, M., Kosmalska, A.J., Oria, R., Kechagia, J.Z., Rico-Lastres, P., Le Roux, A.-L., et al. (2017). Force Triggers YAP Nuclear Entry by Regulating Transport across Nuclear Pores. Cell *171*, 1397–1410.e14.

Fleming, B.M., Yelin, R., James, R.G., and Schultheiss, T.M. (2013). A role for Vg1/Nodal signaling in specification of the intermediate mesoderm. Development *140*, 1819–1829.

Giancotti, F.G., and Ruoslahti, E. (1999). Integrin signaling. Science *285*, 1028–1032.

Goldammer, H., Hollergschwandtner, E., Elisabeth, N.H., Frade, P.R., and Reipert, S. (2016). Automatized Freeze Substitution of Algae Accelerated by a Novel Agitation Module. Protist *167*, 369–376.

Halder, G., Dupont, S., and Piccolo, S. (2012). Transduction of mechanical and cytoskeletal cues by YAP and TAZ. Nat. Rev. Mol. Cell Biol. *13*, 591–600.

Hansen, C.G., Moroishi, T., and Guan, K.-L. (2015). YAP and TAZ: a nexus for Hippo signaling and beyond. Trends Cell Biol. *25*, 499–513.

Kim, N.-G., and Gumbiner, B.M. (2015). Adhesion to fibronectin regulates Hippo signaling via the FAK-Src-PI3K pathway. J. Cell Biol. *210*, 503–515.

Lai, E.C. (2004). Notch signaling: control of cell communication and cell fate. Development *131*, 965–973.

Maître, J.-L., Berthoumieux, H., Krens, S.F.G., Salbreux, G., Jülicher, F., Paluch, E., and Heisenberg, C.-P. (2012). Adhesion functions in cell sorting by mechanically coupling the cortices of adhering cells. Science *338*, 253–256.

Marlow, F.L., and Mullins, M.C. (2008). Bucky ball functions in Balbiani body assembly and animal-vegetal polarity in the oocyte and follicle cell layer in zebrafish. Dev. Biol. *321*, 40–50.

Meng, Z., Qiu, Y., Lin, K.C., Kumar, A., Placone, J.K., Fang, C., Wang, K.-C., Lu, S., Pan, M., Hong, A.W., et al. (2018). RAP2 mediates mechanoresponses of the Hippo pathway. Nature *560*, 655–660.

Miesfeld, J.B., and Link, B.A. (2014). Establishment of transgenic lines to monitor and manipulate Yap/Taz-Tead activity in zebrafish reveals both evolutionarily conserved and divergent functions of the Hippo pathway. Mech. Dev. *133*, 177–188.

Miesfeld, J.B., Gestri, G., Clark, B.S., Flinn, M.A., Poole, R.J., Bader, J.R., Besharse, J.C., Wilson, S.W., and Link, B.A. (2015). Yap and Taz regulate retinal pigment epithelial cell fate. Development *142*, 3021–3032.

Montague, T.G., and Schier, A.F. (2017). Vg1-Nodal heterodimers are the endogenous inducers of mesendoderm. eLife *6*, 178.

Morita, H., Grigolon, S., Bock, M., Krens, S.F.G., Salbreux, G., and Heisenberg, C.-P. (2017). The Physical Basis of Coordinated Tissue Spreading in Zebrafish Gastrulation. Dev. Cell *40*, 354–366.e4.

Nair, S., Lindeman, R.E., and Pelegri, F. (2013). In vitro oocyte culture-based manipulation of zebrafish maternal genes. Dev. Dyn. *242*, 44–52.

Nishioka, N., Inoue, K., Adachi, K., Kiyonari, H., Ota, M., Ralston, A., Yabuta, N., Hirahara, S., Stephenson, R.O., Ogonuki, N., et al. (2009). The Hippo signaling pathway components Lats and Yap pattern Tead4 activity to distinguish mouse trophectoderm from inner cell mass. Dev. Cell *16*, 398–410.

Pan, X., Hobbs, R.P., and Coulombe, P.A. (2013). The expanding significance of keratin intermediate filaments in normal and diseased epithelia. Curr. Opin. Cell Biol. *25*, 47–56.

Perrimon, N., Pitsouli, C., and Shilo, B.-Z. (2012). Signaling mechanisms controlling cell fate and embryonic patterning. Cold Spring Harb. Perspect. Biol. *4*, a005975.

Porazinski, S., Wang, H., Asaoka, Y., Behrndt, M., Miyamoto, T., Morita, H., Hata, S., Sasaki, T., Krens, S.F.G., Osada, Y., et al. (2015). YAP is essential for tissue tension to ensure vertebrate 3D body shape. Nature *521*, 217–221.

Rauzi, M., Verant, P., Lecuit, T., and Lenne, P.-F. (2008). Nature and anisotropy of cortical forces orienting Drosophila tissue morphogenesis. Nat. Cell Biol. *10*, 1401–1410.

Saxton, R.A., and Sabatini, D.M. (2017). mTOR Signaling in Growth, Metabolism, and Disease. Cell *168*, 960–976.

Schindelin, J., Arganda-Carreras, I., Frise, E., Kaynig, V., Longair, M., Pietzsch, T., Preibisch, S., Rueden, C., Saalfeld, S., Schmid, B., et al. (2012). Fiji: an open-source platform for biological-image analysis. Nat. Methods *28*, 676–682.

Selman, K., Wallace, R.A., Sarka, A., and Qi, X. (1993). Stages of oocyte development in the zebrafish, Brachydanio rerio. J. Morphol. *218*, 203–224.

Wang, L., Luo, J.-Y., Li, B., Tian, X.Y., Chen, L.-J., Huang, Y., Liu, J., Deng, D., Lau, C.W., Wan, S., et al. (2016). Integrin-YAP/TAZ-JNK cascade mediates atheroprotective effect of unidirectional shear flow. Nature *540*, 579–582.

Westerfield, M. (2007). The Zebrafish Book: A Guide for the Laboratory Use of Zebrafish (Danio Rerio), Fourth Edition (Univ. of Oregon Press).

Yanagimachi, R., Cherr, G., Matsubara, T., Andoh, T., Harumi, T., Vines, C., Pillai, M., Griffin, F., Matsubara, H., Weatherby, T., and Kaneshiro, K. (2013). Sperm attractant in the micropyle region of fish and insect eggs. Biol. Reprod. *88*, 47.

Yu, F.-X., Zhao, B., and Guan, K.-L. (2015). Hippo Pathway in Organ Size Control, Tissue Homeostasis, and Cancer. Cell *163*, 811–828.

Zanconato, F., Forcato, M., Battilana, G., Azzolin, L., Quaranta, E., Bodega, B., Rosato, A., Bicciato, S., Cordenonsi, M., and Piccolo, S. (2015). Genome-wide association between YAP/TAZ/TEAD and AP-1 at enhancers drives oncogenic growth. Nat. Cell Biol. *17*, 1218–1227.

Zhang, H., Liu, C.-Y., Zha, Z.-Y., Zhao, B., Yao, J., Zhao, S., Xiong, Y., Lei, Q.-Y., and Guan, K.-L. (2009). TEAD transcription factors mediate the function of TAZ in cell growth and epithelial-mesenchymal transition. J. Biol. Chem. *284*, 13355–13362.

STAR★METHODS

KEY RESOURCES TABLE

REAGENT or RESOURCE	SOURCE	IDENTIFIER
Antibodies		
Cytokeratin 18 Antibody (RGE53) monoclonal Ab	Thermo (Invitrogen)	Cat#MA1-06326; RRID: AB_559772
YAP and TAZ (D24E4) rabbit monoclonal Ab	Cell Signaling	Cat#8418; RRID: AB_10950494
Fibronectin (H-300) rabbit polycolonal Ab	Santa Cruz	Cat#sc-9068; RRID: AB_2105699
Laminin rabbit polycolonal Ab	Sigma	Cat#L9393; RRID: AB_477163
Integrin beta-1 rabbit polycolonal Ab	Chemicon	Cat#AB1952; RRID: AB_91150
Phospho-S6 Ribosomal Protein (Ser235/236) rabbit polycolonal antibody	Cell Signaling	Cat#2211S; RRID: AB_331680
Anti-Notch1 intracellular domain rabbit polycolonal Ab	Abcam	Cat#ab8387; RRID: AB_306525
Anti-Tubulin, Acetylated mouse monoclonal	Sigma-Aldrich	Cat#T6793; RRID: AB_477585
Alexa Fluor 350 goat anti-rabbit IgG (H+L)	Thermo Fisher Scientific	Cat#A-21068; RRID: AB_2535729
Alexa Fluor 488 goat anti-mouse IgG (H+L)	Molecular Probes	Cat#A-11029; RRID: AB_138404
Alexa Fluor 488 goat anti-rabbit IgG (H+L)	Molecular Probes	Cat#A-11008; RRID: AB_143165
Alexa Fluor 546 goat anti-mouse IgG (H+L)	Molecular Probes	Cat#A-11003; RRID: AB_141370
Alexa Fluor 546 goat anti-rabbit IgG (H+L)	Molecular Probes	Cat#A-11010; RRID: AB_143156
Alexa Fluor 647 goat anti-mouse IgG (H+L)	Molecular Probes	Cat#A-21235; RRID: AB_141693
Alexa Fluor 647 goat anti-rabbit IgG (H+L)	Molecular Probes	Cat#A-21244; RRID: AB_141663
Chemicals, Peptides, and Recombinant Proteins		
EDTA	Sigma	Cat#ED-500G; CAS: 60-00-4
RGD (Arg-Gly-Asp)	Abcam	Cat#ab142698; CAS: 99896-85-2
cRADfC	Peptides international	Cat#PCA-3960-PI; CAS: 1055991-02-0
cRGDfC	Peptides international	Cat#PCA-3686-PI; CAS: 862772-11-0
FAK inhibitor 14	Sigma	Cat#SML0837; CAS: 4506-66-5
PF-573228	Sigma	Cat#PZ0117; CAS: 869288-64-2
Dasatinib	Sigma	Cat#CDS023389; CAS: 302962-49-8
SCH772984	Abmole	Cat#M2084; CAS: 942183-80-4
LY294002	Selleckchem	Cat#S1105; CAS: 154447-36-6
Wortmannin	Selleckchem	Cat#S2758; CAS: 19545-26-7
BX-795	Sigma	Cat#SML0694; CAS: 702675-74-9
OSU-03012 (AR-12)	Selleckchem	Cat#S1106; CAS: 742112-33-0
MK-2206 2HCl	Abmole	Cat#M1837; CAS: 1032350-13-2
GSK690693	Selleckchem	Cat#S1113; CAS: 937174-76-0
Rapamycin	Selleckchem	Cat#S1039; CAS: 53123-88-9
DAPT	Sigma	Cat#D5942; CAS: 208255-80-5
Experimental Models: Organisms/Strains		
Zebrafish: *AB wild-type*		N/A
Zebrafish: *wwtr1*^{mw49}	Miesfeld et al., 2015	RRID: ZFIN_ZDB-GENO-160122-7
Zebrafish: *yap1*^{mw48}	Miesfeld et al., 2015	RRID: ZFIN_ZDB-GENO-160122-3
Zebrafish: *buc*^{p106re}	Marlow and Mullins, 2008	RRID: ZFIN_ZDB-GENO-140612-10
Zebrafish: Tg(krt18:krt18-GFP)	Gift from Masazumi Tada (University College London, UK)	N/A
Zebrafish: Tg(krt4:EGFP-CAAX)	Morita et al., 2017	ZFIN ID: ZDB-TGCONSTRCT-111207-1
Zebrafish: Tg(buc:buc-EGFP)	Bontems et al., 2009	ZFIN ID: ZDB-TGCONSTRCT-151209-1

(*Continued on next page*)

Continued

REAGENT or RESOURCE	SOURCE	IDENTIFIER
Software and Algorithms		
Fiji	Schindelin et al., 2012	https://fiji.sc/
Imaris	Bitplane	http://www.bitplane.com/imaris
Excel	Microsoft	https://products.office.com/en-US/
GraphPad Prism	GraphPad Software	https://www.graphpad.com/scientific-software/prism/

CONTACT FOR REAGENT AND RESOURCE SHARING

Further information and requests for resources and reagents should be addressed to and will be fulfilled by the Lead Contact, Carl-Philipp Heisenberg (heisenberg@ist.ac.at).

EXPERIMENTAL MODEL AND SUBJECT DETAILS

Fish maintenance and embryo collection were carried out as described (Westerfield, 2007). 5-24 months old females from WT AB strains, as well as *Tg(krt18:krt18-GFP)*, *Tg(krt4:EGFP-CAAX)*, *Tg(buc:buc-EGFP)*, *wwtr1*^{mw49}, *yap1*^{mw48}, *buc*^{p106re} zebrafish lines were used in this study. Fish were bred in the zebrafish facility at IST Austria according to local regulations, and all procedures were approved by the Ethic Committee of IST Austria regulating animal care and usage.

METHOD DETAILS

Ovarian Follicle Isolation

Methods of ovarian follicle isolation and culture were adapted from (Elkouby and Mullins, 2017; Nair et al., 2013). Female fish were anesthetized in 0.02% Tricaine, and euthanized by decapitation. Ovaries were harvested in culture medium [70% Leibovitz's L-15 medium with L-glutamine, pH 8.0 (GIBCO), Penicillin-Streptomycin 50 U/ml, and 0.5% bovine serum albumin (BSA, Sigma-Aldrich)]. Follicles were isolated from ovaries by gentle pipetting with a glass Pasteur pipette and dissection with forceps. Stage II to early stage III (100-400 μm diameter) follicles were kept in culture medium for up to 4 days at 26°C.

Scanning Electron Microscopy

For high pressure freezing (HPF), living follicles were incubated with 10% BSA in culture medium, placed in cup-shaped aluminum platelets with a 200 μm indentation (Engineering Office M. Wohlwend GmbH, Switzerland) and covered with flat platelets. The oocytes were fast frozen using a HPM 010F (Bal-TEC, Switzerland). Following HPF, the carriers were carefully transferred with a liquid nitrogen filled shuttle into tubes containing 1% osmium tetroxide/0.2% uranyl acetate in 97% acetone/3% water on dry ice. The tubes were then placed in the freeze substitution (FS) device (Leica Microsystems GmbH, EM AFS2, Austria) and set to the following parameters: T1 = −90°C for 6 h, S1 = 15°C, T2 = −60°C for 3 h, S2 = 15°C, T3 = −30°C for 3 h, S3 = 15°C, T4 = 4°C for 1 h. To speed up the FS we inserted a module for sample agitation in the cryochamber of the AFS2 (Goldammer et al., 2016). After FS, samples were washed 3x10min with ice cold acetone, subsequently infiltrated on ice with different proportions of resin (hard Durcupan/acetone, 1:2, 1:1, 2:1, one hour each) and infiltrated in pure resin overnight at RT. Finally the aluminum platelets carrying the samples were transferred to BEEM capsules, filled with fresh resin and polymerized for 48 h at 60°C. Afterward the resin around the aluminum platelets was trimmed and the cured blocks were dipped in liquid nitrogen. The platelets were then carefully detached using a razorblade with the follicles remaining at the surface of the resin block. The blocks were trimmed with an Ultratrim diamond knife (Diatome, Switzerland) to a rectangle (1.5 × 1 mm) and a depth of 100 μm using an ultramicrotome (Leica Microsystems GmbH, EM UC7, Austria). Prior to serial sectioning, a carbon-coated 8 mm wide Kapton tape (RMC Boeckeler, USA) was plasma treated using an ELMO glow discharge cleaning system (Agar Scientific, UK), equipped with a homemade reel-to-reel motorized winder, for increasing the hydrophilicity of the tape. Serial ultrathin sections of 70 nm thickness were cut with a 4 mm Ultra 35° diamond knife (Diatome, Switzerland) and picked up with the plasma-treated tape using an automated tape-collecting ultramicrotome ATUMtome (RMC Boeckeler, USA). After collecting the sections on the tape, it was cut into strips and mounted on 4 inch silicon wafers (University Wafer, USA) with conductive double sided adhesive carbon tape (Science Services, Germany). The wafers were then coated with a 5 nm carbon layer to ensure conductivity (Leica Microsystems GmbH, EM ACE600, Austria). Sections were imaged by a scanning electron microscope (FE-SEM. Merlin compact VP, Carl Zeiss, Germany) equipped with the Atlas 5 Array Tomography software (Carl Zeiss, Germany). The high-resolution serial images for 3D-SEM reconstruction (Figure 1G) were taken with 5 nm pixel resolution, and for showing intermediate filaments (Figures 1B–1D) were 2.5 nm, at 5kV using a backscattered electron detector.

Brigh-field Imaging

Brigh-field images of whole embryos and chorion/micropyle were taken on a Leica M165 FC stereo-microscope.

Phalloidin, DAPI and Immunohistochemistry

After isolation, follicles were fixed in a glass vial containing freshly-prepared 70% Leibovitz's L-15 medium with 0.05% BSA and 3.7% formaldehyde adjusted to pH8.0 at 4°C over night. For staining embryos at 90% epiboly stage (Figure S2A), embryos were fixed in PBS containing 3.7% paraformaldehyde at 4°C over night. After fixation, samples were washed 6 × 10 min in PBS with 0.1% Triton X-100, permeabilized by PBS with 0.5% Triton X-100 for 2 h at room temperature, and blocked in PBS containing 0.5% Triton X-100 and 5% goat serum for 4 h at room temperature. The samples were then incubated in primary antibodies dissolved 1:300 in blocking buffer at 4°C over night, and washed 3 × 10 min in PBS with 0.1% Triton X-100. Incubation with secondary antibodies and Phalloidin-Rhodamine was performed as described for the primary antibodies. For DAPI staining, samples were incubated in a 1:500 dilution for 30 min at room temperature.

Confocal Imaging

Samples were mounted in 0.4% low-melting-point (LMP) agarose (VWR), and imaged on an inverted or upright Zeiss LSM 880 confocal microscope equipped with a Zeiss LD C-Apochromat 40x/1.1 W Corr M27 lens. Images were rendered using Imaris (Bitplane) and processed using FIJI.

Analysis of Cell Volume and Area versus Height Value

SEM images were aligned and segmented manually with Fiji TrakEM2. SEM and confocal image data were 3D reconstructed with Imaris using the surface function. All SEM cell surfaces were generated automatically. For confocal microscopy data, nucleus and MPC surfaces were automatically generated based on DNA and TAZ/Krt18 antibody staining, while the granulosa cell surface was semi-automatically generated based on Phalloidin and Krt18 staining. The cell volume was automatically determined with Imaris based on cell surface segmentation. For measuring the area versus height ratio, first a reference axis of the analyzed cell was assigned oriented perpendicular to the surface of the oocyte beneath this cell. The area of the analyzed cell was defined as the projected planar cell area oriented perpendicular to the reference axis. The height of the analyzed cell was defined as the projected length along the reference axis.

Analysis of Fluorescent Intensity

TAZ nucleus versus cytoplasm intensity ratio was defined as the mean intensity ratio of nuclear to cytoplasmic TAZ signals. The mean intensity value of nuclear TAZ was automatically determined by Imaris based on nuclear surface segmentation. The mean intensity of cytoplasmic TAZ was determined by dividing the total cytoplasmic TAZ intensity by the cytoplasm volume. Nuclear NICD intensity was determined as described for TAZ. Krt18, Integrin, Phospho-S6, Fibronectin, Laminin and pAKT antibody staining intensities for the MPC were analyzed by calculating the mean intensity value in the MPC region on single sections from z stack confocal images with FIJI. For determining MPC versus granulosa cell Krt18 intensity ratio, granulosa cell Krt18 staining intensity was calculated as described for the MPC but within a restricted region (30 μm) surrounding the MPC. For determining Krt18-GFP/F-actin intensity ratio, a line of 10 pixel width (1.76 μm) was drawn on single sections from z stack confocal images, oriented perpendicularly to individual junctions between granulosa cells using FIJI. Fluorescent signals in the Krt18 and F-actin channels were plotted and analyzed along this line. The peak values of the two channels were then used to calculate the intensity ratio.

Analysis of Granulosa Cell Density and Number

When measuring cell density (Figures S5F–S5H), nuclei segmentation was performed for cells located at the animal pole of the follicle within a region with a maximum depth of 50 μm (labeled as h) from the surface of the animal pole. The surface area of the segmented region was calculated by $2\pi Rh$ with R being the follicle radius. For estimating the total number of follicle cells, the cell density obtained at the animal pole was projected to the entire surface of follicle assuming that cell density is largely uniform within the follicle.

Tissue Tension Measurements

Tension of cell-cell junctions between granulosa cells was assessed by conducting laser ablation with a previously described ultraviolet-laser cut set up (Behrndt et al., 2012) equipped with a Zeiss C-Apochromat 63x/1.2 W Korr UV-VIS-IR lens using Tg(*buc:-buc-GFP*)(*krt18:krt18-GFP*) follicles. For cutting, follicles were mounted in 0.4% LMP agarose (VWR) in culture medium inside a glass-bottom Petri dish (Willcowells). Taking advantage of Buc-GFP expression as a marker of the vegetal pole, follicles were oriented with their animal pole close to the glass-bottom. Laser cuts were performed on single cell-cell junction oriented perpendicular to the MPC, by applying 25 ultraviolet pulses at 1,000 Hz to 6 equidistant sites along a 3 μm long line. Fluorescent images were acquired with an iXon DU-897-BV camera (Andor Technology) using exposure time of 150 ms and 150 ms frame rates. Laser cuts lasted for 0.45 s during which no images were acquired. Before or after acquiring the recoil images, a z stack reference image was taken to determine the position of the junction relative to the MPC. We assessed the initial recoil velocity upon junction cutting as previously described (Rauzi et al., 2008), specifically we generated a kymograph displaying the krt18-GFP signal along the junction versus time (Figure 1L and 1M), and determined the opening slope during the first 120 frames (18 s) after the cut.

Cell Ablation Experiments

Laser ablation of MPC and granulosa cells was performed by multiple UV laser cuts in the nuclear region of the targeted cells using the same laser cutting setup as described for the tissue tension measurements. For short-term cultures, late stage II (270-330 μm) follicles were used, and for long-term MPC re-specification experiments, early-middle stage II (190-230 μm) follicles were used. For MPC ablation experiments, follicles were chosen that showed a single specified MPC, as judged by the expression of Krt18-GFP. MPC ablation efficiency was determined by observing Krt18-GFP expression in granulosa cells at the oocyte animal pole at 6h - 24h after ablation. Ablated follicles were incubated in culture medium at 26°C in individual agarose molds to avoid cross-contamination, and the culture medium was replaced every 12h.

Follicle Aspiration Experiments

Follicle aspiration experiments were performed as previously described (Maître et al., 2012). Before aspiration, 45 μm glass pipettes (BioMedical Instruments) with 30° bent angle were passivated with 5% BSA in culture medium for 20 min at RT. The micropipettes were then connected to a Microfluidic Flow Control System (Fluigent, Fluiwell), with negative pressure ranging from 7-750 Pa. The microfluidic setup was mounted on two micromanipulators (Eppendorf, Transferman NK2). Micropipette movement and pressure were controlled via a custom-programmed Labview (National Instruments) interface. For aspiration of the animal pole containing the MPC and surrounding granulosa cell, late stage II Tg(*buc:buc-GFP*) follicles were used. After aspiration for 1.5 h, follicles were directly fixed by adding 40% formaldehyde into the medium up to a final concentration of 4%. Follicles were removed from the aspiration pipette with forceps after 2 min of preliminary fixation, and transferred to a glass vial containing freshly prepared 70% Leibovitz's L-15 medium with 0.05% BSA and 3.7% formaldehyde adjusted to pH8.0 for further fixation at 4°C over night.

Drug Treatments

Follicles were incubated in culture medium with 10 - 100 mM EDTA for 3 h or 9 h, or with 2 mg/ml RGD peptides or inhibitors for 8 h at 26°C. The following inhibitor concentration were used: FAK inhibitor 14, 250 μM; PF-573228, 10 μM; Dasatinib, 5 μM; SCH772984, 1 μM; LY294002, 50 μM; Wortmannin, 2 μM; BX-795, 10 μM; OSU-03012, 10 μM; MK-2206, 5 μM; GSK690693, 5 μM; and Rapamycin, 10 μM; DAPT 100 μM. After incubation, follicles were fixed in a glass vial containing freshly prepared 70% Leibovitz's L-15 medium with 0.05% BSA and 3.7% formaldehyde adjusted to pH8.0 at 4°C over night.

QUANTIFICATION AND STATISTICAL ANALYSIS

Statistical analysis of data was performed with Excel and GraphPad Prism 7 software. Unpaired Mann-Whitney *U* tests were used to calculate two-tailed *P value*s. Sample size and *P value*s are mentioned within the figures and legends.

Supplemental Figures

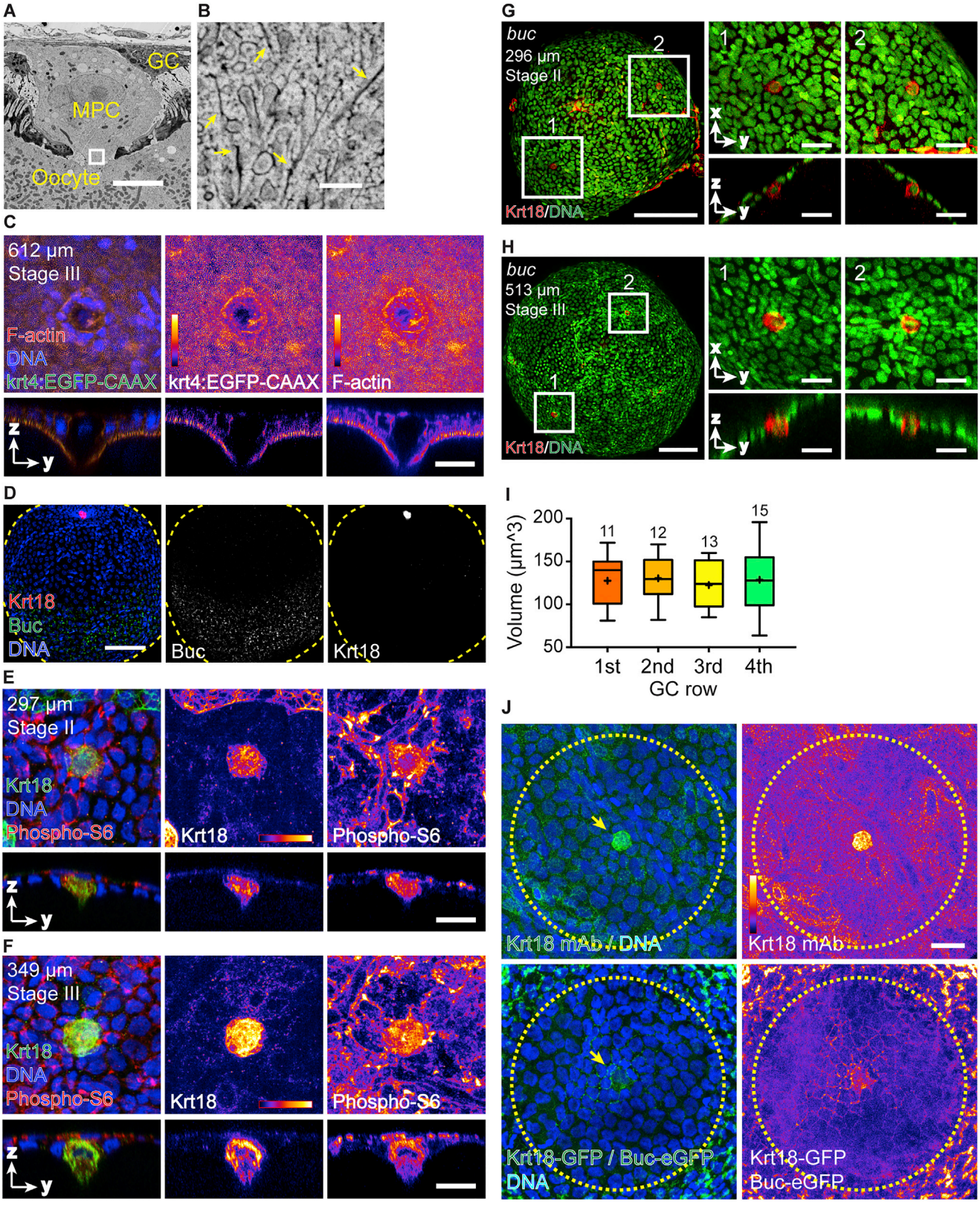

(legend on next page)

Figure S1. Characterization of MPC, Related to Figure 1

(A) Scanning electron microscopy (SEM) image of a MPC at stage II (318 μm diameter). Scale bar, 5 μm.

(B) High magnification view of the boxed area outlined in (A). Yellow arrows point at filamentous structures with a diameter of ≈ 25 nm found in the protrusion of the MPC directed towards the oocyte, indicative of microtubule accumulation within the protrusion. Scale bars, 0.3 μm.

(C) Confocal images of MPC and granulosa cells at the animal pole of stage III follicles. Cell nuclei are marked by DAPI, F-actin by Phalloidin-Rhodamine, and Krt4 transcription by transgenic krt4:EGFP-CAAX. Follicle maturation stages are indicated by follicle diameter in the upper left corner. Upper panels are maximum intensity projection (MIP) planar x,y views and lower panels are y,z cross-sections along a horizontal line passing through the center of the MPC. Scale bars, 25 μm.

(D) MIP confocal images of a stage III follicle. Vegetal pole is labeled by transgenic Buc-GFP expression, cell nuclei by DAPI, and Krt18 by immunohistochemistry. Dashed line indicate outline of the follicle. Scale bar, 100 μm.

(E and F) Confocal images of MPC and granulosa cells at the animal pole of stage II (E) and III (F) follicles. Cell nuclei are marked by DAPI, and Krt18 & Phospho-S6 by immunohistochemistry. Follicle maturation stages are indicated by follicle diameter in the upper left corner. Upper panels are MIP planar x,y views and lower panels are y,z crosssections along a horizontal line passing through the center of the MPC. Scale bars, 15 μm.

(G and H) Confocal images of MPC specification (marked by Krt18 expression) in stage II (G) and III (H) follicles from *buc* homozygous females. Cell nuclei are marked by DAPI, and Krt18 by immunohistochemistry. Left panel shows global view of the follicle. Stages of follicle maturation are indicated by follicle diameter in the upper left corner. Boxed areas demarcate different MPCs and their surrounding region. Scale bars, 100 μm. Middle and right panels are high magnification views of the boxed areas outlined in left panel; upper panels are MIP planar x,y views and lower panels are y,z cross-sections along a horizontal line passing through the center of the MPC. Scale bars, 20 μm.

(I) Volume of granulosa cells in the first 4 cell rows surrounding the MPC obtained from confocal microscopy images (Figure 1J) of late stage II follicles. Color-coding of the plot boxes refers to color-coding of the cell rows in (Figure 1J, right column). Values are shown as Tukey box-and-whisker plots with median (bar) and average values (cross). Sample size (cells) is indicated over each box; data are from 4 follicles of 2 animals.

(J) MIP confocal images of Krt18 expression at the animal pole of middle stage II follicles. Cell nuclei are marked by DAPI. Krt18 is labeled by either immunohistochemistry (upper row) or transgenic Krt18-eGFP expression (lower row). Yellow arrows indicate MPC, and dashed yellow line outlines animal pole region. Green fluorescent signal outside the dashed circle (animal pole) in lower panels shows transgenic Buc-eGFP expression at the vegetal pole. Note that the weak Krt18 signal detected by Krt18-GFP expression in granulosa cells surrounding the MPC in the lower right panel can also be detected by Krt18 immunohistochemistry (upper panels) but is not clearly distinguishable from background staining in the overlying theca cell layer and the oocyte. Scale bars, 20 μm.

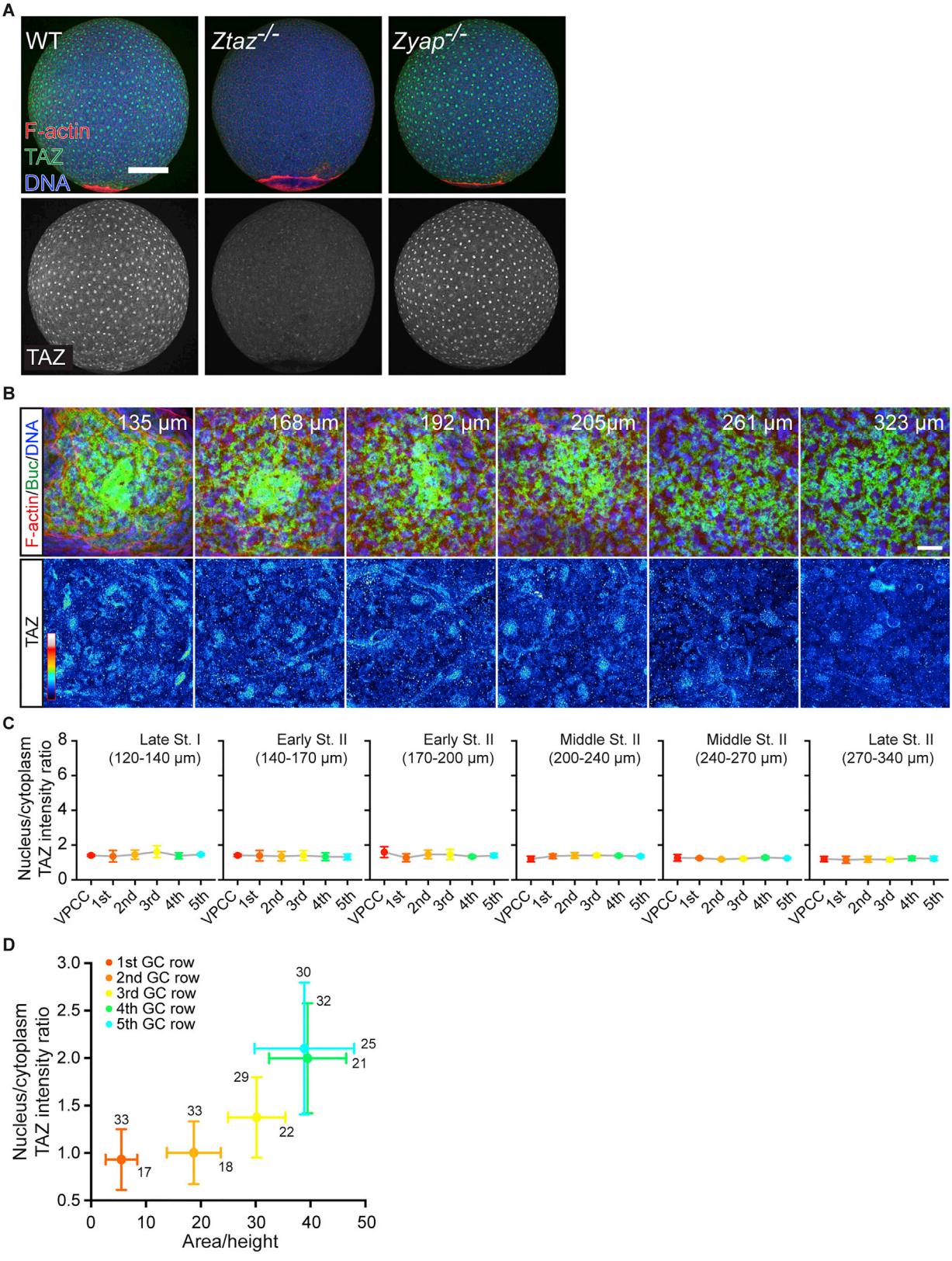

(legend on next page)

Figure S2. Inverse Correlation between Granulosa Cell Deformation by MPC and Nuclear TAZ Accumulation, Related to Figure 2

(A) Maximum intensity projection (MIP) confocal images of WT, zygotic taz homozygous, and zygotic yap homozygous embryos. Cell nuclei are marked by DAPI, F-actin by PhalloidinRhodamine, TAZ by immunohistochemistry. TAZ immunoreactivity is significantly reduced in taz homozygous but not yap homozygous embryos. Scale bar, 150 μm.

(B) MIP confocal images of cells at the vegetal pole of stage I-II follicles with the cell cortex labeled by Phalloidin-Rhodamine, cell nuclei by DAPI, Buc by Buc-eGFP expression (upper row), and TAZ (lower row) by immunohistochemistry. Stages of follicle maturation are indicated by follicle diameter in the upper right corner. Scale bar, 15 μm.

(C) Nuclear-to-cytoplasmic TAZ intensity ratio in granulosa cells at the center of the vegetal pole (vegetal pole center cells, VPCC) and surrounding granulosa cells (GCs) of stage I-II follicles. Values are shown as mean (dot) and standard deviation (whisker). Data are from 3 follicles for late stage I (120-140 μm), 3 for early stage II (140-170 μm), 4 for early stage II (170-200 μm), 4 for middle stage II (200-240 μm), 3 for middle stage II (240-270 μm), and 8 for late stage II (270-340 μm); follicles were collected from 3 animals. From each follicle around 80 cells were analyzed.

(D) Plot of area to height ratio (x axis) versus nucleus/cytoplasm TAZ intensity ratio (y axis) of granulosa cells (GCs) in different rows surrounding the MPC obtained from confocal images. Values are shown as average values (round dots) and standard deviation (whiskers). Color-coding of dots refers to color-coding of the cell rows in (Figure 1J). Sample size (cells) is indicated over each whiskers; data are from 10 late stage II follicles of 3 animals.

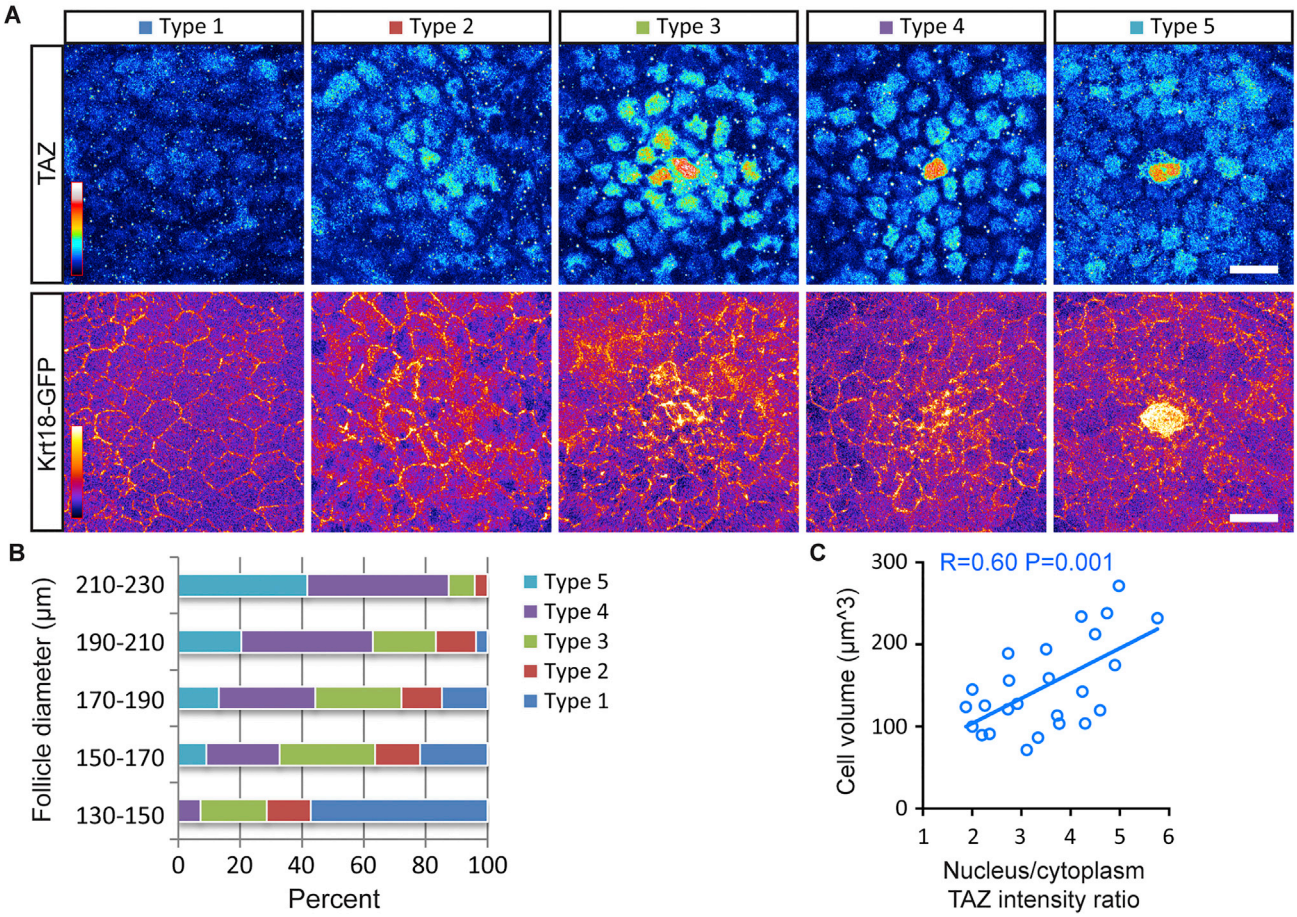

Figure S3. Selection of a Single MPC Is a Stepwise Process, Related to Figure 2

(A) Maximum intensity projection (MIP) confocal images of MPC and granulosa cells at the animal pole of early-middle stage II follicles. Follicles are sorted into 5 distinct TAZ localization patterns (Type 1-5). TAZ is labeled by immunohistochemistry and Krt18 by transgenic Krt18-eGFP expression. Scale bars, 15 μm.

(B) Distribution of Type 1-5 TAZ localization patterns for follicles during consecutive stages of maturation between late stage I and middle stage II. Data are from 14 (130-150 μm), 55 (150-170 μm), 61 (170-190 μm), 54 (190-210 μm) and 24 (210-230 μm) follicles of 25 animals.

(C) Plot of cell volume as a function of nucleus/cytoplasm TAZ intensity ratio in Type 3 follicles, when a small group of granulosa cells at the animal pole begins to express higher levels of TAZ than their immediate neighbors. Data are from 6 follicles of 3 animals. Linear regression analysis was performed; coefficient of correlation (R) and P value (P) are shown.

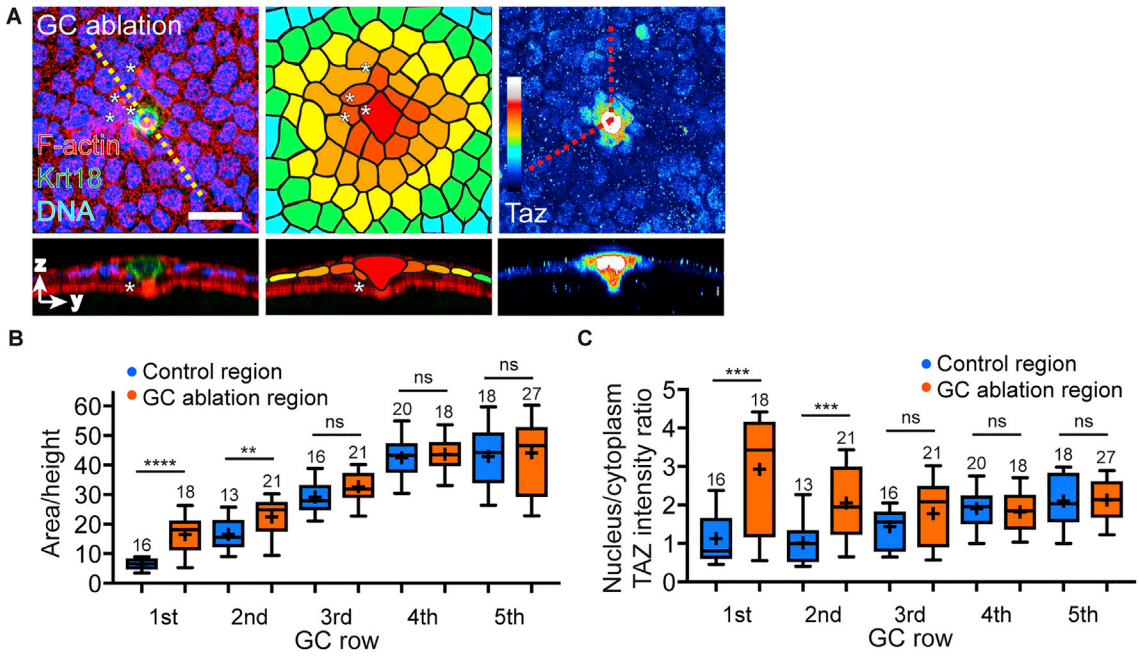

Figure S4. Granulosa Cell Ablation Relieves Remaining Granulosa Cells Compaction and Restores Nuclear TAZ Accumulation, Related to Figure 3

(A) Confocal images (left and right column) and image segmentation (middle column) of cells at the animal pole of late stage II follicles after laser ablation of several granulosa cells directly adjacent to the MPC. Samples are fixed at 6 h after laser ablation. MPC is labeled by transgenic Krt18-GFP expression, cell nuclei by DAPI and TAZ by immunohistochemistry. Upper row is maximum intensity projection (MIP) planar x,y view, and lower row is y,z cross-section along the yellow dashed line in left column. White stars demarcate ablated granulosa cells, which were typically extruded from the granulosa layer toward the oocyte. In right column, the remaining granulosa cells surrounding the MPC are binned into two sector regions depending on their distance to the ablated granulosa cells. In the representative image, the region in up-left corner is considered as the ablation region, while the other parts are considered as the non-ablated control region. Scale bar, 20 μm.

(B and C) Area to height ratio (B) and nucleus to cytoplasm TAZ intensity ratio (C) of granulosa cells in the control and ablation regions outlined in (A). Values are shown as Tukey box-and-whisker plots with median (bar) and average values (cross). Sample size (cells) is indicated over each box; data are from 6 late stage II follicles of 3 animals (for control and GC ablation experiments each). Statistical test, Mann-Whitney *U* test, two tailed. ns, not significant; **P < 0,01; ****P < 0.0001.

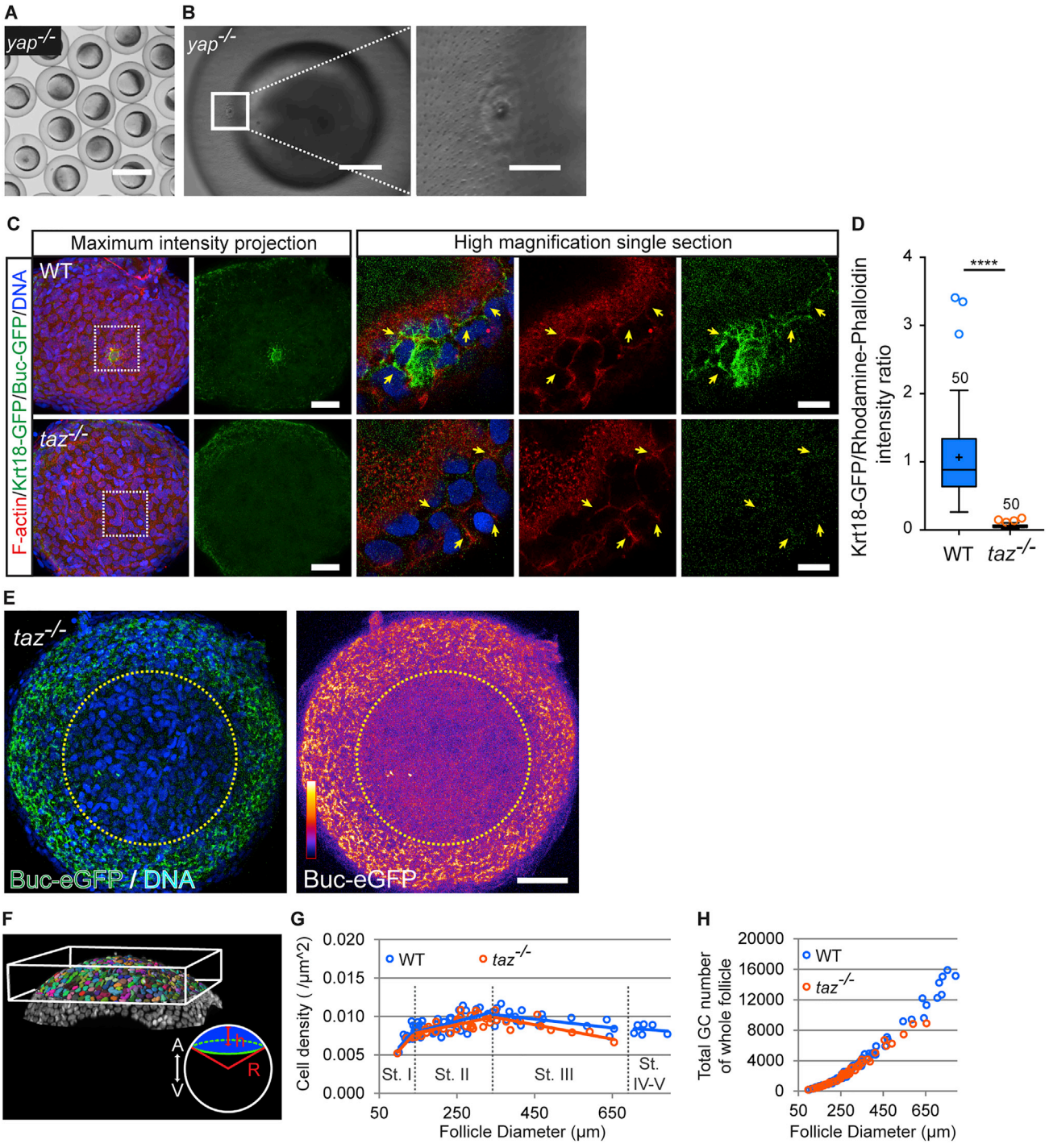

Figure S5. TAZ Activity Is Dispensable for Oocyte Polarization and Granulosa Cell Proliferation during Early Stages of MPC Specification, Related to Figure 5

(A) Bright-field image of embryos generated by yap homozygous females crossed with WT males. Scale bar, 1 mm.

(B) Bright-field images of the micropyle region within the chorion of an embryo generated by yap homozygous females crossed with WT males. Left panel is low magnification view of the chorion with the micropyle region outlined by white box (left panel). Scale bar, 200 μm. Right panel is high magnification view of the boxed region in the left panel showing the micropyle. Scale bar, 50 μm.

(C) Maximum intensity projection (MIP) confocal images (left two columns) and high magnification single section confocal images (right three columns, boxed area in the columns on the left) of MPC and granulosa cells at the animal pole of middle stage II follicles. Cell nuclei are marked by DAPI, F-actin by Phalloidin-

(legend continued on next page)

Rhodamine and Krt18 by transgenic Krt18-eGFP expression. Animal pole is defined as the center of the granulosa cell layer lacking Buc-GFP signal at the vegetal pole. Yellow arrows point at co-localization between Krt18 and F-actin. Scale bars, 30 μm (left two columns) and 10 μm (right three columns).

(D) Krt18-GFP/Phalloidin-Rhodamine intensity ratio in granulosa cells at the animal pole of middle stage II follicles. Values are shown as Tukey box-and-whisker plots with median (bar) and average values (cross). Sample size (lines) is indicated over each box; data are from 3 middle stage II follicles (200-270 μm diameter) of 2 animals (for WT and taz homozygous experiments each). Statistical test, Mann-Whitney U test, two tailed. ****$P < 0.0001$.

(E) MIP confocal images of a late stage II follicle from taz homozygous female. Cell nuclei are marked by DAPI. The transgenic Buc-eGFP signal (vegetal pole marker) is still restricted to the area outside the dashed circle (animal pole), similar as in WT (Figure S1C). Scale bars, 50 μm. (F) Nuclei segmentation was performed in cells located at the animal pole of the follicle within a region with maximum depth of 50 μm (labeled as h) from the surface of the animal pole. R indicate sphere radius of the follicle. Surface area of the segmented region equals to $2\pi Rh$.

(G) Cell density as a function of follicle diameter and thus follicle maturation within the segmented region as outlined in (C) in WT and taz mutant follicles shown. n (WT), 49 follicles from 5 animals; n (taz-/-), 32 follicles from 3 animals.

(H) Total granulosa cell (GC) number as a function of follicle diameter and thus follicle maturation in wild type and taz mutant follicles n (WT), 49 follicles from 5 animals; n (taz-/-), 32 follicles from 3 animals.

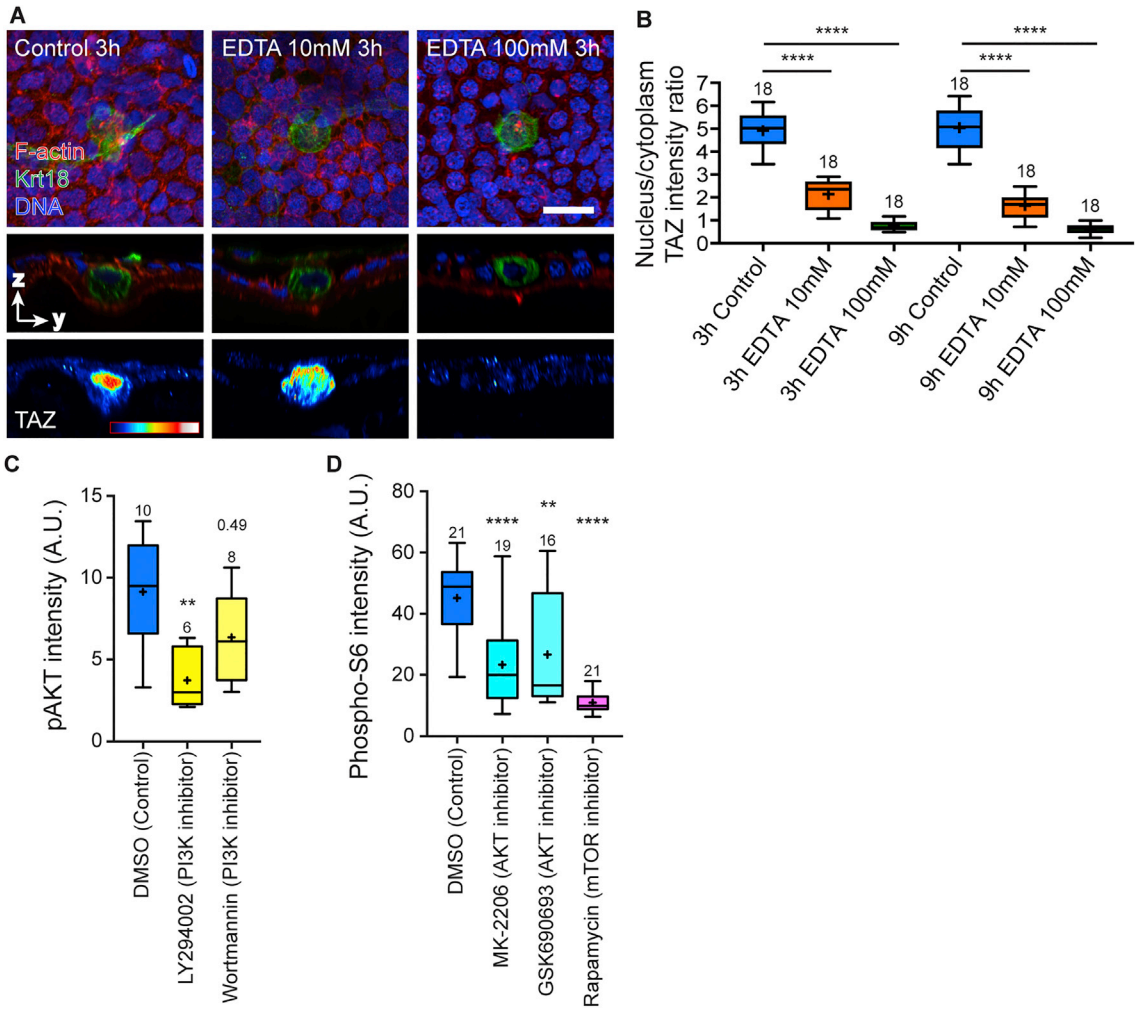

Figure S6. TAZ Activity in MPC Depends on Cell-Matrix Adhesion, Related to Figure 7

(A) Confocal images of MPC and granulosa cells at the animal pole of stage II follicles exposed to either 10 mM or 100 mM EDTA for 3 h. Cell cortex is marked by Phalloidin-Rhodamine labeled F-actin, cell nuclei by DAPI, Krt18 and TAZ by immunohistochemistry. Upper panels are maximum intensity projection (MIP) planar x,y views, and panels in the two rows below are y,z cross-sections along a horizontal line passing through the center of the MPC. Scale bar, 15 μm.

(B) Nucleus to cytoplasm TAZ intensity ratio in MPC exposed to EDTA for 3 or 9 h. Values are shown as Tukey box-and-whisker plots with median (bar) and average values (cross). Sample size (cells) is indicated over each box; data are from 108 late stage II follicles of 8 animals. Statistical test, Mann-Whitney U test, two tailed. **** $P < 0.0001$.

(C and D) Phospho-AKT (Ser473, to evaluate PI3K inhibitor efficiency, C) and Phospho-S6 (Ser235/236, to evaluate AKT and mTOR inhibitor efficiency, D) staining intensity in MPC after exposure to DMSO (control) or indicated inhibitors. Values are shown as Tukey box-and-whisker plots with median (bar) and average values (cross). Sample size (cells) is indicated over each box; data are from middle-late stage II follicles of 2 (C) and 4 (D) animals. Statistical test was performed between each treatment group and the DMSO control, Mann-Whitney U test, two tailed. Non-significant P values are indicated above the sample size; **$P < 0.01$; ****$P < 0.0001$.

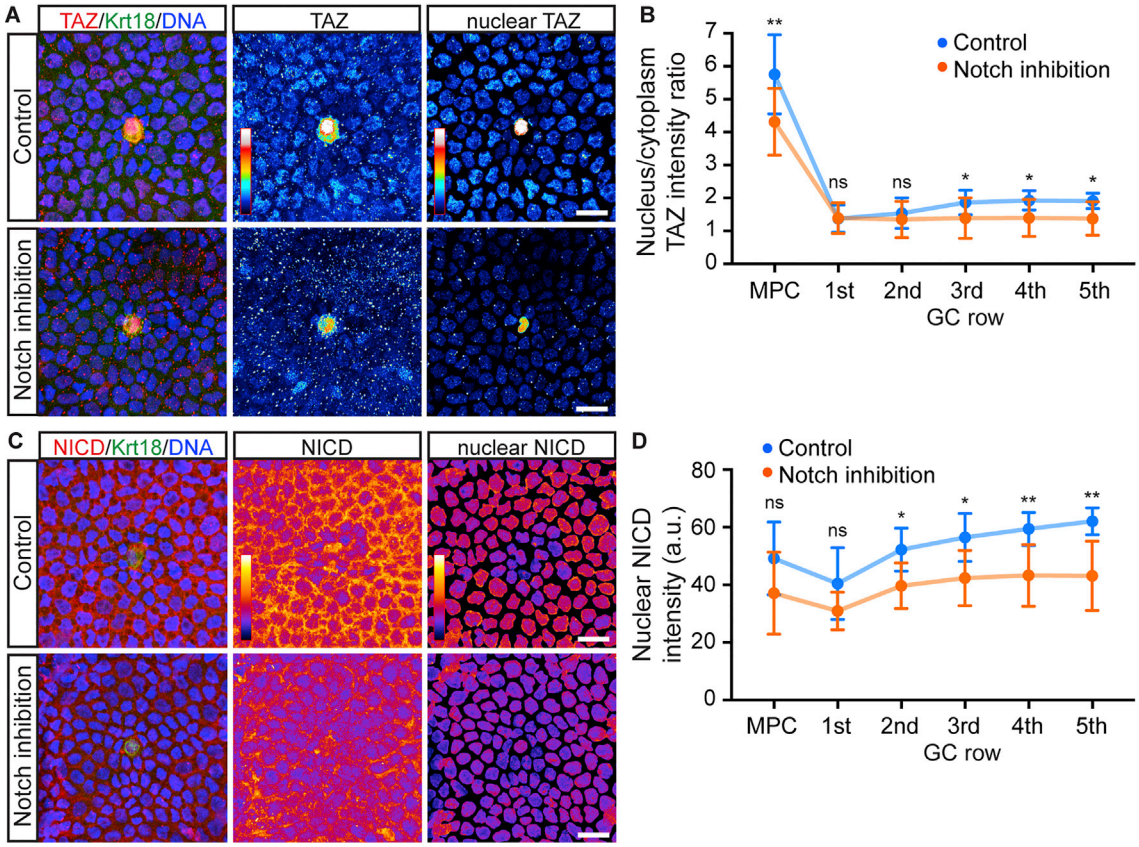

Figure S7. Lateral Inhibition during MPC Specification Is Not Mediated by Notch Signaling, Related to Figure 7

(A) Maximum intensity projection (MIP) confocal images of TAZ localization in MPC and granulosa cells at the animal pole of late stage II follicles exposed to DMSO (control) or DAPT (100 μM, 8 h). Cell nuclei are marked by DAPI, Krt18 by transgenic Krt18-eGFP expression, and TAZ by immunohistochemistry. Confocal images (left and middle column) and nuclei segmentation (right column) were shown. Scale bars, 15 μm.

(B) Nucleus to cytoplasm TAZ intensity ratio in MPC and surrounding granulosa cells (GCs) exposed to DMSO (control) or DAPT (100 μM, 8 h). Values are shown as mean (dot) and standard deviation (whisker). Data are from 15 (control) and 11 (DAPT) middle-late stage II follicles (200-340 μm diameter) of 3 animals. For each follicle around 80 cells were analyzed. Statistical test, Mann-Whitney U test, two tailed. ns, not significant; *P < 0,05; **P < 0.01.

(C) Maximum intensity projection (MIP) confocal images of Notch intracellular domain (NICD) in MPC and granulosa cells at the animal pole of middle-late stage II follicles exposed to DMSO (control) or 100 μM DAPT (γ-secretase inhibitor) for 8 h. NICD is labeled by immunohistochemistry with an antibody targeting Notch1 intracellular domain, cell nuclei by DAPI, and Krt18 by transgenic Krt18-eGFP expression. Confocal images (left and middle column) and nuclei segmentation (right column) were shown. Scale bars, 15 μm.

(D) Nuclear NICD intensity in MPC and surrounding granulosa cells (GCs) exposed to DMSO (control) and DAPT (100 μM, 8 h). Values are shown as mean (dot) and standard deviation (whisker). Data are from 8 (control) and 6 (DAPT) middle-late stage II follicles (200-340 μm diameter) of 3 animals. For each follicle around 80 cells were analyzed. Statistical test, Mann-Whitney U test, two tailed. ns, not significant; *P < 0,05; **P < 0.01.